GEOLOGICAL SETTING AND GEOCHEMICAL SIGNATURES OF THE MAFIC ROCKS FROM THE INTRA-PONTIDE SUTURE ZONE: IMPLICATIONS FOR THE GEODYNAMIC RECONSTRUCTION OF THE MESOZOIC NEOTETHYS

Kaan Sayit[1], Michele Marroni[2, 3], M. Cemal Göncüoglu[1], Luca Pandolfi[2, 3], Alessandro Ellero[3], Giuseppe Ottria[3] and Chiara Frassi[2]

[1] Department of Geological Engineering, Middle East Technical University, Ankara, Turkey.
[2] Dipartimento di Scienze della Terra, Università di Pisa, Italy.
[3] Istituto di Geoscienze e Georisorse, CNR, Pisa, Italy.

==

CORRESPONDING AUTHOR:
PROF. MICHELE MARRONI,
DIPARTIMENTO DI SCIENZE DELLA TERRA,
UNIVERSITÀ DI PISA, VIA S. MARIA, 53
56126 PISA, ITALY.
E-MAIL: marroni@dst.unipi.it

ABSTRACT

A number of suture zones exist in Turkey, which is believed to represent the closure of Paleo and NeoTethyan oceanic basins. Regarding the development of the latter oceanic entity, namely Neotethys, the geodynamic evolution of the Intra-Pontide branch, the northernmost one of a number of oceanic basins remains enigmatic. The Intra-Pontide Suture Zone (IPSZ) in Northwest Turkey includes several tectonic units most of which are characterized by the occurrence of mafic rocks with distinct geochemical signatures. In this paper, the mafic rocks collected from four of these units (the Domuz Dağ Unit, the Saka Unit, the Daday Unit and the Arkot Dağ Mèlange) have been studied in detail along two selected transects.

The Domuz Dağ Unit is characterized by amphibolites, micaschists and marbles, which have been overprinted by low-grade metamorphism.The Saka Unit is in turn represented by an assemblage of slices of amphibolites, marbles and micaschists metamorphosed under upper amphibolite facies metamorphic conditions in the Late Jurassic time. In these units, the amphibolites and their retrograded counterparts display E-MORB-, OIB-BABB- and IAT-type signatures. The Daday Unit is characterized by metasedimentary and metamafic rocks metamorphosed under blueschist to sub-greenschist facies conditions. The metamafic rocks comprise actinolite-bearing schists and Na-amphibole-bearing varieties possibly derived from basaltic and gabbroic protoliths. They have a wide range of chemical compositions, displaying N-MORB-, E-MORB-, OIB- BABB- and IAT-type signatures. The Arkot Dağ Mèlange consists of a Late Santonian assemblage of slide-blocks mainly represented by basaltic lithologies showing affinities ranging from N-MORB- and IAT- to BABB-type magmas.

The geochemical signature of the studied mafic rocks indicates that the tectonic units documented along the two studied transects of the Intra-Pontide Suture Zone have been derived from a supra-subduction zone. This hypothesis corroborates the available data collected from the Aylı Dağ Ophiolite Unit cropping out in the westernmost studied transect. This finding can provide new insights for the reconstruction of the geodynamic history of the Intra-Pontide domain.

Key word: mafic rocks, ophiolites, geochemistry, Intra-Pontide Suture Zone, Turkey,

INTRODUCTION

The alpine collisional belts of the Eastern Mediterranean area are characterized by an assemblage of continental terranes separated by several numbers of suture zones (e.g. Göncüoğlu et al. 1997). The Anatolia peninsula is one of the best examples of this structural setting, where each of the suture zones, in fact, was derived by the convergent-related processes that have affected both the oceanic basins and the neighboring continental margins. As a result, each suture zone consists of an assemblage of variably deformed and metamorphosed continental and oceanic units, including: ophiolite sequences (derived from different geodynamic settings), magmatic arc fragments, ophiolite-bearing mélange and successions representative of the continental margins.

Several suture zones are identified in Turkey, which are generally believed to represent the closure of Tethyan ocean basins (e.g. Şengör and Yılmaz 1981). Of these, the Intra-Pontide suture (IPS) zone (Şengör and Yılmaz 1981; Göncüoğlu et al. 1987; Yılmaz 1990; Göncüoğlu and Erendil 1990; Yılmaz et al. 1995; 1997; Okay and Tüysüz 1999; Elmas and Yiğitbaş 2001; Robertson and Ustaömer 2004; Göncüoğlu et al. 2008; Robertson and Ustaömer 2011) is the less studied one. There is very poor data available on this suture zone, mainly about its eastern outcrops. As a consequence, despite its importance for the geodynamic reconstruction of the Eastern Mediterranean area during the Mesozoic-Early Tertiary time, its geodynamic evolution is thus poorly understood.

Since the geochemical signatures of the mafic rocks contain important clues about the tectonic setting from which they have originated (e.g. Pearce 1983; Condie 2005; Sayit et al. 2010), they represent an important tool for the geodynamic reconstruction. These geochemical fingerprints can provide important information about the occurrence of different types of oceanic basins, the development of a magmatic arc or the presence of rifting-related magmatism (e.g. Saccani et al. 2003; Göncüoğlu et al. 2012). The petrogenetic implications derived from a geochemical study may also be important to correlate or compare mafic rocks that have experienced distinct metamorphic conditions. Since the geochemical signatures reflect the nature of protolith, they are better indicators to trace the origin than the degree of metamorphism.

In this study, we present a detailed geochemical study on mafic rocks from the eastern sector of the IPS zone along the Boyali - Daday and Tosya - Emirköy transects. The collected data and their comparison with data on mafic rocks of the surrounding areas are discussed in order to provide a reconstruction of the geodynamic evolution of the IPS zone.

OVERVIEW OF THE MAFIC ROCKS FROM THE INTRA-PONTIDE SUTURE ZONE

The geological setting of the Anatolia can be described as an assemblage of continental microplates enclosed between the margins of the Eurasian plate to the north, and the Afro-Arabian plate to the south (Fig. 1). All these microplates are separated by ophiolite-bearing suture zones of different ages that mark the areas where the PaleoTethyan and NeoTethyan oceanic basins were destroyed by the subduction and/or obduction processes since the Late Paleozoic time (e.g. Okay and Whitney 2010). Among these suture zones, the IPS zone is regarded as the boundary between the Istanbul-Zonguldak (IZ) and Sakarya (SK) composite terranes, extending more than 400 km between Northwest and Central Turkey (Şengör et al. 1980; Tüysüz 1990; Robertson and Ustaömer 2004, Göncüoğlu et al. 2008) (Fig. 1). The IZ terrane overlays the assemblage of oceanic and continental units of IPS zone, which, in turn, are thrust onto the SK terrane (Şengör and Yılmaz 1981; Okay et al. 1996; Okay 2000), an about 1500 km long and 120 km wide fragment made up of a number of oceanic and continental units.

The IZ terrane crops out as an about 400 km long and 70 km wide belt, located to the north of the IPS zone at the southwestern margin of the Black Sea (Fig.1). This terrane includes a Neoproterozoic basement unconformably overlain by a very thick, continuous sedimentary sequence of Ordovician to Carboniferous age, which is only weakly deformed during the Variscan orogeny (e.g. Görür et al. 1997). The non-metamorphic Paleozoic sequence of Zonguldak Unit of the IZ terrane is in turn unconformably overlain by a thick sequence of Late Permian-Paleocene sedimentary deposits, also including Late Cretaceous andesite-bearing volcanoclastic sediments.

The SK terrane (i.e. the Sakarya continent of Şengör and Yılmaz 1981) is represented by a Variscan continental basement tectonically coupled with a variably deformed and metamorphosed Triassic subduction/accretion complex known as the Karakaya Complex (Tekeli 1981; Okay et al. 1996; Okay 2000; Okay and Göncüoğlu 2004). The deformation and the metamorphism documented in the Karakaya Complex occurred in the Latest Triassic as result of the "Cimmerian orogenesis" which may have resulted from the north-dipping subduction of the PaleoTethys oceanic lithosphere below the Laurasia continental margin (e.g. Robertson and Ustaömer 2012). Alternatively, this orogenic event may be linked to a southerly subducting Paleotethys beneath the northern margin of Gondwana (e.g. Göncüoğlu et al. 2000; Sayit and Göncüoğlu 2013). The Karakaya Complex is unconformably covered by a non-metamorphic Early Jurassic – Middle Paleocene sedimentary cover, whose upper part is represented by foredeep deposits known as Tarakli Flysch (Catanzariti et al. 2013).

The IPS zone can be depicted as an assemblage of continental and oceanic units, each with different age, metamorphic imprint and deformation history (Figs. 2 and 3). This assemblage includes ophiolite sequences, ophiolite-bearing mélanges and slices of metamorphic rocks, probably derived from a wide domain including the Intra-Pontide Oceanic (IPO) basin.

Despite their importance, the geochemical data from the mafic rocks from the IPS zone are scarce. Some of these data, however, are accompanied by precise age findings and hence have provided crucial information on the tectono-magmatic evolution of the IPO basin. To the East of Bolu, for example, a huge slide block of basalt in the Arkot Dağ Mélange (Göncüoğlu et al. 2008) is associated with the Late Jurassic cherts and displays MORB-like signatures. Another tight constraint comes from the Ayli Dağ Ophiolite located to the north of Araç town. Here, the basalts interbedded with Middle Jurassic cherts show affinities to BABB-type magmas generated at oceanic back-arc systems whereas IAT-type basalts also exist, but they occur in subordinate amounts. BABB- and IAT-type signatures have also been reported from a slide-block within the Arkot Dağ Mélange (Göncüoğlu et al. 2014). Apart from these studies focusing on the ophiolitic assemblages, the previous work on the geochemistry of the metamorphic rocks comes from the study of Ustaomer and Robertson (1999). These authors reported IAT-, MORB- and WPB-type signatures from the low-grade metamorphic unit defined as the "Domuzdağ-Saraycikdağ Complex" which is partially equivalent to the Daday Unit in the present study.

THE BOYALI-DADAY AND TOSYA – EMIRKÖY TRANSECTS

In Central Turkey, the easternmost segment of the IPS zone is well exposed along two north-south trending transects, hereafter referred to as Boyalı-Daday and Tosya-Emirköy transects (Fig. 1). The first transect runs from the Boyalı to Daday villages across the

Ayli Dağ Mountain and the Araç valley (Fig. 2), whereas the second transect starts from the north of Tosya town and continues northward across the Ilgaz Mountains up to the Emirköy village (Fig. 3).

In both transects, the IPS zone consists of an imbricate stack of different tectonic units, including metamorphic rocks, ophiolites as well as slices of mélange (Fig. 4).

The Early Eocene sedimentary deposits of the Safranbolu - Karabük Basin seal the relationships among the IPS units cropping out in the Araç and Kara valleys (e.g., Yigitbas et al. 1999). These deposits are exposed in the Araç Valley along the Boyali-Daday transect, whereas in the Tosya-Emirköy transect the Eocene succession has been recognized north of the Cebeci village. Thus, the development of the imbricate stack can be regarded in both transects as the result of pre-Eocene thrusting events affecting the different units of IPS zone that are already deformed (Catanzariti et al. 2013).

Concerning the metamorphic units, field evidences (i.e. the occurrence of clasts of foliated and metamorphic rocks within the Eocene deposits) indicate that the ductile deformations as well as the metamorphic imprints predate the sedimentation of the Early Eocene deposits (Okay et al. 2013; Marroni et al. 2014).

Moreover, since Miocene the multiple events of transpression and transtension related to the North Anatolian Fault (NAF) have strongly reworked the original structural setting of the imbricate stack of the IPS zone. These events produced sub-vertical strike-slip faults and low-angle reverse faults that cross cut both the boundaries of the different units of IPS zone and the Eocene deposits (Şengör et al. 2005; Ellero et al. 2015).

In the study areas, the imbricate stack of the IPS zone consists of six distinct tectonic units: the Aylı Dağ Ophiolite (e.g. Göncüoğlu et al. 2012), the Arkot Dağ Mélange (e.g. Göncüoğlu et al. 2014) and four metamorphic units, referred to as Emirköy (Ballidağ-Küre; Yiğitbaş et al. 1999), Daday (Göncüoglu et al. 2014), Saka (Okay et al. 2006; cfr. Devrekani Unit of Göncüoglu et al. 2014 and Marroni et al. 2014) and Domuz Dağ Units (Ustaömer and Robertson 1993; Okay et al. 2006) (Fig. 5). A correlation chart with the previous literature based on both metamorphic/lithological features and location in the geological maps is shown in table1.

This imbricate stack is probably the result of several episodes of out-of-sequence thrusts that affected the whole IPS zone. The imbricate stack is thrust over the sedimentary cover of the Sakarya Terrane, whose top is represented by the Tarakli Flysch of Late Cretaceous-Middle Paleocene age (Catanzariti et al. 2013). The units from IPS zone are, in turn, topped by the klippen of the IZ terrane as recognized west of the Siragomu town (Fig. 2).

Non-metamorphic volcanic rocks, mainly andesites occur within slices along the NAF in the both the investigated transects. These slices consist of a sequence of lava flows (both massive and pillow lava) and volcanoclastic sediments. The lava flow is generally alternated with matrix-supported volcanoclastic breccia levels. This sequence shows a transition to carbonate turbidites consisting of beds of limestone, marlstone and shales. Volcanoclastic arenites are found interlayered with the carbonate turbidite. These successions can be correlated with the Campanian-Maastrichtian Yaylacay and Yaprakli Formations of Rice et al (2006).

The detailed analyses of the relationships among the different units of the IPS zone allow to create a reconstruction of the pristine tectonic relationships among the different tectonic units. This reconstruction includes the metamorphic units showing at its top the Arkot Dağ Mélange and the ophiolite unit (Fig. 4).

The four metamorphic units are characterized by different metamorphic histories. It must be noted, however, that the definition and distribution of these metamorphic units differs between previous studies, which makes a direct correlation with literature impossible. Because of this, Göncüoğlu et al. (2014) had chosen the name Devrekani Unit for the higher-grade metamorphic units, which included different tectonostratigraphic entities, such as the Saka and Domuzdağ Complexes of Okay et al. (2013), Elekdağ and Karakaya Units of Tüysüz (1990) and Kargi and Domuzdağ-Saraycik Complexes of Ustaömer and Robertson (1993). However, to differentiate this unit from the homonymous metamorphic rocks to the Northwest of Kastamonu and because of priority reasons we preferred to change the name of this unit to Saka Unit.

The Domuz Dağ Unit has been recognized in the Tosya-Emirköy transect (Figs. 3 and 5) where it widely crops out mainly in the northern sectors. This unit has been originally defined by Okay et al. (2006) as an assemblage of quartz-mica schists, metabasites, marbles, quarzites and metaserpentinites. The metabasites range from eclogites to garnet- and glaucophane-bearing amphibolites and albite- and chlorite bearing schists. The eclogite inlayers found in the metaserpentinites from the northern areas show the peak conditions at 490 ± 20°C and 1.7 ± 0.02 GPa that took place in the Early Cretaceous on the basis of ^{40}Ar-^{39}Ar age dating (~105 Ma, Okay et al. 2006). In this paper, the name Domuz Dağ Unit is used with a broader sense, according to the prevalence in the study area of marbles, micaschists and amphibolites (Fig. 6a and b), the latters with or without glaucophane. These rocks as well as the eclogites underwent to a retrograde metamorphic path under P and T conditions typical of greenschist facies metamorphism (Okay et al. 2006). The Domuz Dağ unit records a polyphase deformation history very similar to what is documented in the Saka Unit. The last three deformational phases occurred under retrograde metamorphism ranging from greenschist to very low-grade metamorphic conditions.

The outcrops of the Saka Unit have been identified along the Boyalı-Daday transect (Figs 2 and 5) only in three localities (cf. the Saka complex of Okay et al. 2013). It is always sandwiched between the ophiolites of the Ayli Dağ Ophiolite unit or the Arkot Dağ Mélange and the Daday Unit. Along this transect, this unit is not thicker than 300 m. It is represented by garnet-bearing amphibolites, coarse-grained banded amphibolites, garnet-bearing micaschists and coarse-grained impure marble (Fig. 6c and d). The Saka unit records a polyphase deformation history that includes four phases (D1-D4). This resulted in a complex structural setting, as recognized in all the studied outcrops, where the lithologies are folded together since the D2 deformational phases. The polyphase deformation history developed under decreasing P and T conditions. The metamorphic peak documented in the garnet-bearing amphibolites, occurred at temperatures of ~600°C and pressure of 0.80–0.99 GPa (Marroni et al. 2014) during Late Jurassic (~163 Ma: ^{40}Ar-^{39}Ar dating, Marroni et al. 2014). The garnet-bearing amphibolites underwent a retrograde metamorphism ranging from greenschists to sub-greenschist facies conditions (Marroni et al. 2014).

The Daday Unit (cf. the Kargi complex of Okay et al. 2006) in both Boyalı-Daday and Tosya-Emirköy (Figs. 2,3 and 5) transects consists of slices of fine-grained actinolite-bearing schists, fine-grained marbles, paragneisses, mica-bearing schists and black quartzites (Fig. 6e and f). Around the Tuzakli Dam (Fig. 2) the Daday unit (partly corresponding to the Martin, Esenler and Domuzdag Complexes of Okay et al. 2013) is represented by a succession of sandstones, shales, limestones and lydites associated with mafic rocks. Detrital zircon geochronology indicates a Valanginian-Aptian age for this succession (Okay et al. 2013). The Daday Unit is characterized by a complex deformation history analogous to that recognized in the Saka and Domuz Dağ Units recording four pre-Eocene phases, from D1 to D4. This deformation history has developed under retrograde P and T metamorphic conditions from blueschist to sub-greenschist metamorphic facies conditions. The ^{40}Ar-^{39}Ar dating indicates that the metamorphic peak occur between 102 and 112 Ma (Early Cretaceous; Okay et al. 2013).

The Emirköy Unit (Figs. 2, 3 and 5) consists of a monotonous succession of metaturbidites represented by alternating layers of fine-grained metasandstones, metasiltstones and metapelites. This unit is somewhat similar to the turbidite-dominated Martin Complex of Okay et al. (2013), but reflects lower grade metamorphism. In this sense, the Emirköy Unit may represent the deformed and slightly metamorphosed part of the Cağlayan Formation (Okay et al. 2013). It must be noted, however, that the magmatic rocks commonly observed in the Çağlayan Formation have not been found in the Emirköy Unit. The polyphase, pre-Eocene deformation history recognized in this unit includes three deformational phases. Only the first one is characterized by syn-kinematic recrystallization of minerals indicative of very low-grade metamorphic conditions.
On the whole, the field evidences indicate that the Emirköy Unit seems to be represented by a coherent succession of turbidite deposits, whereas the other three metamorphic units show a different tectonic setting, being characterized by an assemblage of up to 100 m thick slices of different lithotypes affected by the same deformational and metamorphic history (e.g. Marroni et al. 2014 for the Saka Unit from the Daday area). In this frame (Fig. 7), the mafic rocks generally occur as huge slices or as few meters thick boudins into the metasedimentary rocks. In both the occurrences the mafic rocks have been found as bodies bounded by shear zones whose attitude is parallel to the main foliation recognized inside the different lithotypes. This structural setting suggests that the metamorphic units represent tectonic mélanges originated in a subduction zone as suggested by their metamorphic grade ranging from blueschist to high-pressure amphibolite and eclogite metamorphic facies (Okay et al. 2006; 2013; Marroni et al. 2014).
The Arkot Dağ Mélange (Figs. 2, 3 and 5) can be depicted as an assemblage of slide-blocks, with different sizes and lithologies, enclosed in a sedimentary matrix consisting of shales, coarse-grained arenites, pebbly-mudstones and pebbly-sandstones (Göncüoğlu et al. 2014). The volume of matrix is generally much less than that of the slide-blocks. Locally the matrix is completely absent. The slide-blocks, ranging in size from few meters to several hundred square meters, show a great variability in their lithological composition, including sedimentary, metamorphic and ophiolite rocks. The ophiolitic rocks include peridotites, gabbros and basalts. In addition slide blocks of the Middle Triassic to Late Cretaceous cherts, Late Jurassic to Early Cretaceous neritic and pelagic limestones, dolostones, Late Cretaceous marly-limestones and ophiolite-bearing arenites, gneisses and micaschists are also found. Moreover, the slide blocks show deformations

developed before their inclusion into the mélange. The source area of the Arkot Dağ Mélange can be thus envisioned as an imbricate stack of deformed and metamorphosed oceanic- and continental-derived slices (Göncüoğlu et al. 2014). The age of the Arkot Dağ Mélange can be ascribed to the Late Santonian on the basis of the nannofossil assemblage recognized in some soft clasts of marls.

The Ayli Dağ Ophiolite crops out in both the studied transects (Figs. 2, 3 and 5). It is mainly composed of slices of serpentinized peridotites, not thicker than 200-300 m, with bands of dunites and pyroxenites. However, in the Ayli Dağ area south of Siragömü village, an almost complete ophiolite sequence has been identified (Göncüoğlu et al. 2012). Its lower part is made up of a mantle sequence of peridotites thick less than 3 km topped by 500-600 m-thick layered gabbros alternating with dm- to m-thick layers of spinel-bearing dunites, melatroctolites, troctolites, ol-gabbros and leucogabbros. The gabbro sequence is overlain by a sheeted dyke complex that passes upward to 100-200 m-thick massive basaltic lava flows followed by 600-800 m-thick massive and pillow lavas and breccias alternating with ophiolite-bearing arenites and cherts. The radiolarian cherts sampled from the top of the pillow lavas yielded radiolarian assemblages indicating the middle Bathonian to early Callovian ages. In addition, an about 10 m thick section of banded amphibolites at the base of the serpentinized peridotites have been found in the Pelitoren area, 500 m west of the Pelitoren village (Fig. 2). According to their relationships with the peridotites, these amphibolites can be interpreted as belonging to a metamorphic sole originated during the obduction of the ophiolites.

GEOCHEMISTRY OF MAFIC ROCKS

In this section, we present new geochemical data obtained on 32 samples from the mafic lithologies of the Daday, Saka and Domuz Dağ units and also from the slide blocks of the Arkot Dağ Mélange. In order to provide a more complete picture of the mafic rocks from IPSZ, the geochemical data from the slide blocks of basalts from the Arkot Dağ Mélange (Göncüoğlu et al. 2014) and mafic lithologies from the Ayli Dağ Ophiolite (Göncüoğlu et al. 2012) have also been taken into account. Analyses of major elements were determined by inductively coupled plasma emission spectrometry (ICP-ES) and trace elements (including REE) were determined by inductively coupled plasma mass spectrometry (ICP-MS) at the ACME analytical labs (Canada). Analytical precision calculated based on the replicate analyses and standards indicate reproducibility generally better than 5% for most major and trace elements. The geochemical data are given in Table 2.

Assessment of Secondary Processes

As previously mentioned, the Daday, Saka and Domuz Dağ units are variably metamorphic, including greenschists, blueschists and amphibolites. Given this significant range, it is likely that the elemental budget of the samples may have been disturbed due to effects of alteration/metamorphism (e.g. Staudigel et al. 1996). Therefore, it is crucial to use the elements that have remained relatively immobile to make reliable petrogenetic interpretations. When plotted against Zr, the elements of relatively high ionic potential (e.g. Th, Nb, Y, and Ti) display good correlations, attesting their immobile character during post-magmatic processes (Fig. 8). In contrast, the elements of low ionic potential, such as Ba, Rb, K, show scattered distribution, suggesting that their abundances may have been modified by the secondary processes (Fig. 8). This idea is further reinforced by the coherent elemental patterns of HFSE and REE (Fig. 9). Thus, we believe that HFSE and REE have remained largely immobile up to amphibolite facies conditions and represent the elemental compositions of the protolith. The stability of these elements under amphibolitic and even eclogitic conditions has been also shown by some other studies (e.g. Spandler et al. 2004; John et al. 2004).

Geochemical Results

The detailed examination of trace element systematics highlights five main chemical types that display distinct elemental fractionation and/or depletion/enrichment histories. All chemical groups include samples of basaltic composition, and except for one type (Type 3), they all display subalkaline character (Fig. 10).

The first type (Type 1) is represented by a single sample (IPS-10-47) in our dataset and found only in the Daday-type slide block embedded in the Arkot Dağ Mélange. This sample is compositionally similar to N-MORB (Sun and McDonough 1989) and plots close to the unity line on the multi-element diagram (Fig. 9a). The depleted, N-MORB-like nature of this chemical type is reflected by high Zr/Nb (37.1), low Zr/Y (2.6) and Nb/Y (0.07) ratios (Figs. 11 and 12). Also, it exhibits LREE-depleted pattern on a chondrite-normalized diagram ($[Ce/Sm]_N$ = 0.73; N denotes chondrite-normalized based on the values of Sun and McDonough 1989) (Fig. 9b).

The second type (Type 2) has been sampled from the Daday and Domuz Dağ units. This type appears to be more enriched relative to Type 1, as evidenced by the higher absolute abundances observed in most trace elements (Fig. 9a). Type 2 samples display slightly fractionated trace element patterns owing to the enrichment in the more incompatible elements relative to the less compatible ones (Th/Yb = 0.09-0.12, Nb/Yb = 1.0-3.8) (Figs. 9 and 13). The relatively enriched nature of Type 2 is also apparent in its lower Zr/Nb (7.4-34.1), higher Zr/Y and Nb/Y ratios (Figs 11 and 12). Relative to Type 1, Type 2 exhibits relatively flat to slightly LREE-enriched profile ($[La/Sm]_N$ = 0.91-1.62) (Fig. 9b). Another feature to be noted on Type 2 samples is the presence of slight Th-La enrichment over Nb (Th/Nb = 0.07-0.12) when compared to N-MORB (0.05).

The third chemical type (Type 3) is very dissimilar from the rest with its highly enriched chemical composition, possessing OIB-like features (e.g. Sun and McDonough 1989; Chauvel et al. 1992). Type 3 samples are found in the Daday and Saka units and characterized by humped trace element patterns, reflecting marked enrichment in the most incompatible elements (Th/Yb = 0.7-4.7, Nb/Yb = 7.1-42.0) (Figs. 9c and 11). The REE patterns are strongly fractionated, with highly enriched LREE profiles combined with noticeable depletion in HREE is also ($[Ce/Sm]_N$ = 1.6-3.5; ($[Dy/Yb]_N$ = 1.3-2.1) (Fig. 9d). The enriched character of the Type 3 is also evident from low Zr/Nb (4.8-9.0), high Zr/Y (5.5-14.5) and Nb/Y (0.6-3.0) (Figs. 11 and 12). We must also note that some members of this group exhibit slight enrichment in Th over Nb (Th/Nb = 0.06-0.21).

The fourth type (Type 4) has been encountered in all four units, namely Daday, Saka, Domuz Dağ units and Arkot Dağ Mélange. This type displays HFSE distribution largely subparallel to N-MORB (Fig. 9e). However, variable depletion exists in Nb relative to Th and La, causing these samples to have high Th/Nb (0.08-0.38) and La/Nb (1.1-2.8) ratios. Type 4 samples mostly exhibit depleted trace element signatures high Zr/Nb (14.8-65.0), low Zr/Y (1.8-4.4) and Nb/Y (0.04-0.23) ratios (Figs. 11 and 12). On chondrite-normalized diagrams, a majority of this group is characterized by LREE-depleted to flat REE patterns ($[Ce/Sm]_N$ = 0.54-1.50, $[Ce/Yb]_N$ = 0.73-2.09) (Fig. 9f). One sample within this group, however, display some degree of enrichment in LREE over HREE ($[Ce/Sm]_N$ = 1.50).

The fifth chemical type (Type 5) has been sampled from the Daday, Saka and Domuz Dağ units and characterized by highly to extremely depleted signatures, as evidenced by very low absolute abundances of some elements, such as Zr (0.06-0.27 ppm) and Hf (0.05-0.29 ppm) (average N-MORB abundances for Zr and Hf are 74 ppm and 2.05 ppm, respectively) (Figs. 9g and 12). The highly depleted character of this group is also apparent when they are plotted on N-MORB normalized diagrams (Fig. 9g). Some Type 5 samples show negative anomalies in Zr and Hf, whereas one sample displays relative enrichment in these elements. REE patterns of this chemical type appear to be variable; while some Type 5 samples exhibit relatively flat MREE-HREE profile, others display gradual depletion towards MREE. LREE patterns, on the other hand, changes from flat to LREE-enriched ($[Ce/Sm]_N$ = 0.59-2.50) (Fig. 9h).

DATA INTERPRETATION

Trace element ratios of the studied samples vary within a significant range, which cannot simply be explained by post-melting processes, such as fractional crystallization and/or accumulation. Instead, the existence of a number of chemical species with distinct trace element systematics clearly point out a non-uniform origin, which may involve melt generation taking place at more than one tectonic setting and/or contribution from different mantle source regions.

It is generally assumed that the crust-mantle differentiation has resulted in depletion of some part of the mantle due to migration of incompatible elements into the crust. Thus, the depleted mantle (DM) is deficient in incompatible elements with respect to the less incompatible ones, producing high ratios of Zr/Nb (34.2) coupled with low Zr/Y (1.5) and Nb/Y (0.04) (ratios calculated on the basis of the DMM values of Workman and Hart 2005). Among our chemical groups, such signatures are typically observed on Type 1 (Zr/Nb = 37.1) and Type 4 (Zr/Nb avg = 37.9), suggesting that these groups have largely tapped a depleted mantle component.

In contrast to Types 1 and 4, Type 2 samples display in general lower Zr/Nb and higher Zr/Y and Nb/Y, indicating enriched characteristics (Figs. 11 and 12). Note that all Type 2 samples have incompatible trace element concentrations greater than that of N-MORB, thus they stay above the line of unity. Also, almost all Type 2 samples show greater LREE enrichment compared to those from Type 1, as reflected by their higher La/Sm values (Fig. 12). Considering also the gradual enrichment of elements with increasing incompatibility, the trace element systematics of Type 2 samples may suggest greater contribution from enriched sources (so lesser contribution from a depleted source) and/or smaller degrees of partial melting. The greater LREE enrichment seen in two samples may suggest that the involvement of enriched sources has been even greater compared to the other Type 2 samples. However, given the fact that these two samples reflect similar level of enrichment in MREE-HREE patterns, it appears to be more likely that this feature is an artifact of small degrees of partial melting.

The OIB-like trace element signatures of Type 3 samples may reflect the greatest contribution from enriched source(s). This is also evidenced by the low values of Zr/Nb coupled with high Zr/Y and Nb/Y (Figs. 11 and 12). In addition to that, low degrees of partial melting also seem to have played a role in creating the enriched and fractionated trace element patterns of Type 3 samples. It must also be noted that the two samples with the highest degree of enrichment are the ones with least MgO content. This implies that fractional crystallization may have some effect on creating these elevated abundances. The presence of cross-cutting patterns, however, indicates that fractional crystallization may not be the sole control on the trace element systematics of these samples, though we cannot entirely exclude the effect of high-pressure fractionation of garnet (Fig. 9c and d). It seems, therefore, that partial melting and/or the nature of mantle source region may also have influenced the elemental variations of these two samples.

Type 5 displays the most depleted signatures among the studied groups, with very low concentrations in most trace elements (Figs. 10g and 12). These samples, however, display some unusual signatures. We mentioned above that Types 1 and 4 exhibit geochemical signatures (e.g. high Zr/Nb) that reflect their derivation from a mantle source region where DM has been the predominant component. In contrast, Type 5 samples display relative enrichment in Nb (and LREE) compared to Zr and Hf, which leads to moderate Zr/Nb ratios. On the basis of this, this might seem at first that the contribution of DM was probably not too strong, but this is clearly not the case. The trace element signatures apparently more depleted than N-MORB is difficult to reconcile with derivation from a fertile N-MORB source (Fig. 9g). Instead, such depleted characteristics can be attributed to derivation from N-MORB mantle source which has previously experienced melt extraction (e.g. D-DMM, Workman and Hart 2005). It must be noted that three of Type 5 samples have high MgO content (~18-22 wt.%), so olivine accumulation may have been another factor responsible for the low trace element concentrations. However, the other samples from this group have MgO contents around 8 wt.%, thus suggesting that the highly depleted signatures are not solely an artifact of post-melting processes.

On the basis of discussion above it is seen that the studied groups reflect variable contribution depleted/enriched components. It must be noted, however, that almost all Type 4 samples possess negative Nb anomalies, which is a typical feature of magmas generated above subduction zones (e.g. Pearce 1983). The relative depletion in Nb (relative to Th and LREE) is generally attributed to the presence of residual accessory phases in the subducting slab, which leads to selective retention of Nb along with other HFSE (e.g. Green 1995). Other elements, however, are preferentially incorporated into the fluids and/or melts released from the slab and metasomatize the overlying mantle wedge (e.g. Tatsumi and Eggins 1995).

It is also noteworthy that some Type 4 samples attain very high Zr/Nb values, reaching up to 65.0. Such values are well above the average N-MORB value (31.8, Sun and McDonough 1989). To a first order approximation, these high values may indicate the involvement of a pre-depleted DM-type mantle source. However, if we exclude Nb, most Type 4 samples show immobile trace element concentrations similar or higher than N-MORB. This suggests therefore that these samples have mainly tapped a regular DM component. The occurrence of very high values of Zr/Nb, then, requires another explanation. It is previously mentioned that Type 4 samples are variably depleted in Nb. Some Type 4 samples, however, have Nb concentrations relatively depleted with respect to other HFSE. The presence of negative Nb anomalies and the relative depletion of other HFSE relative to LILE and LREE is very typical in arc basalts, which is generally attributed to the presence of residual accessory phases in the subducting slab (e.g. Green 1995). In some cases, however, a mineral phase like rutile may preferentially retain Nb during sediment melting, resulting in distinct fractionation of HFSE (e.g. Class et al. 2000). Thus, we think that very high Zr/Nb values observed on Type 4 samples may have resulted from the selective partitioning taking place during subduction of oceanic lithosphere.

MELTING SYSTEMATICS

The extensive range observed in trace element ratios strongly argue for source heterogeneity and/or varying degrees of partial melting. The source heterogeneity, in turn, may be linked to the involvement of distinct lithological components, such as eclogite/pyroxenite and peridotite (e.g. Allegre and Turcotte 1986; Ito and Mahoney 2005). In this sense, eclogitic oceanic crust and volatile-rich/metasomatized lithosphere represent the enriched streaks embedded in the depleted, dry peridotitic matrix (e.g. Niu and O'Hara 2004; Sayit 2013). The mixing of melts derived from these distinct lithologies can generate a range of trace element and isotopic compositions based on their proportion in the mixture. To a first order approximation, the high Zr/Nb, low Zr/Y and

Nb/Y signatures of Types 1 and 4 can be interpreted as the predominant contribution of the melts deriving from the depleted peridotitic matrix, whereas the relatively more enriched signatures of Type 2 samples may suggest lower degrees of melting and/or that the effect of the depleted peridotite have been diluted to some extent. The highly depleted Type 5 samples, on the other hand, probably involve melt generation from more depleted sources, requiring pre-melt extraction. The OIB-like, Type 3 samples may indicate strong contribution from enriched, readily fusible streaks in association with small-degree melting.

In order to get a general understanding of the influence of partial melting and the mantle source on the geochemical signatures of the samples, we apply two melt modeling schemes (Fig. 13). The first one is ratio-based, including the trace element pairs Sm/Yb and Dy/Yb and used to model Type 1 to 4 samples. It is difficult, however, to infer the melting systematics of Type 5 samples owing to their somewhat unusual trace element systematics. Thus, we apply the second scheme involving absolute Sm concentration, which allows us to better monitor the process of depletion. In our calculations, we use elemental ratios and the samples with greater than 5% MgO to minimize the effects of fractional crystallization. For both models, it is assumed that the melting have occurred in a non-modal fashion (see the figure explanation for the source and melt modes used in the calculations). Melting curves have been modeled according to batch and fractional melting schemes (see the figure for the details). In the calculations, the spi-peridotite source is assumed to have DMM-type composition, representing the depleted matrix, whereas the garnet-peridotite has more enriched, E-DMM-type composition, characterizing the streaks of oceanic lithosphere. Selected partition coefficients are given in Table 2.

On the basis of the first modeling scheme, it can be suggested that Type 1 (N-MORB-like) and Type 2 (E-MORB-like) samples largely appear to have been formed in the stability of spinel and reflect predominant contribution of the depleted material (Fig. 13). The E-MORB-like samples reflect relatively lower degrees of melting compared to the N-MORB-like sample, which is in agreement with their more enriched character. Type 3 (OIB-type) samples, being the most enriched samples in our dataset, appear to have involved low-degree melt fractions deriving from the enriched material. It is noteworthy, however, that most Type 2 samples as well as some Type 4 samples plot in the area between the melting curves of grt-peridotite and spi-peridotite. Such sample compositions can be explained by mixing of melts deriving from these peridotitic sources. Type 3 samples that plot outside the mixing region, on the other hand, probably require different melting systematics, which may be linked to, for example, the modification of the mantle source by previous melt extraction and/or metasomatism by slab-derived melts.

The second modeling scheme suggests clearly that the highly depleted nature of Type 5 samples cannot be explained by melting of asthenospheric N-MORB source and a previous melt extraction is necessary (Fig. 13). On the basis of the model, this pre-depletion process can be achieved by about 25% melting. The re-melting of this source produces Sm/Yb ratios more depleted than the observed values. However, if the pre-depleted source (i.e. the residue after 25% melting) is subsequently metasomatized by low-degree OIB-type melts (~1%), then melting of such source can reproduce the observed compositions.

DISCUSSIONS

TECTONOMAGMATIC CONSTRAINTS

Among the studied sample groups, Type 1 exhibits depleted trace element signatures, resembling to N-MORBs generated at mid-ocean ridges (e.g. Sun and McDonough 1989; Niu et al. 1999). N-MORB-type melts are the common products of the decompression melting of depleted asthenospheric mantle or depleted MORB mantle (DMM) (e.g. Zindler and Hart 1986). The predominant involvement of a depleted mantle source in the petrogenesis of Type 1 samples is also consistent with the modeling results that largely require spi-facies melts deriving from DMM-type mantle. Although N-MORB-like magmas are typically associated with mid-ocean ridges, they have been also reported from intra-oceanic back-arc basins (e.g. Pearce et al. 1995; Leat et al. 2004). The melting systematics in back-arc basins are somewhat similar to those of mid-ocean ridges such that melting is mainly accomplished by adiabatic decompression (e.g. Pearce and Stern 2006). The important difference arises from the fact that the back-arc basin basalts may involve slab-derived components to variable extents in their petrogenesis. In back-arc systems, N-MORB-like melts are generally observed to be constrained to the centers and away from the arc-front (e.g. Pearce and Stern 2006).

In contrast to Type 1, the relatively more enriched, Type 2 samples are more akin to E-MORBs. E-MORB-type magmas are also commonly associated with the mid-ocean ridges, however they are also known to exist in other tectonic settings, such as back-arc basins, seamounts and oceanic islands (e.g. Haase and Devey 1994; Leat et al. 2000;

Chauvel and Hemond 2000). In contrast to N-MORBs, E-MORB-type melts tend to have relatively enriched isotopic signatures, therefore suggesting contribution from a distinct mantle component (e.g. Niu et al. 2001). As noted in the previous section, the enriched component can be characterized by pyroxenitic/eclogitic lithologies and/or enriched peridotite that are dispersed within the depleted peridotitic matrix (e.g. Ito and Mahoney 2005; Sayit 2013). These enriched streaks can be regarded as pieces of oceanic lithosphere that have been recycled and re-introduced into the mantle by plumes (e.g. Hofmann and White 1982; Sayit 2013).

Type 4 samples are distinct with their negative Nb anomalies, which are typical of magmas generated at subduction zones (e.g. Pearce 1983). The relative enrichment of Th and LREE with respect to HFSE implies that Type 4 samples have been derived from a mantle source that was fluxed by slab-derived components. The high Zr/Nb ratios coupled with low Nb/Yb values suggest that Type 4 melts have been generated in an intra-oceanic subduction system (e.g. Pearce and Peate 1995). Trace element systematics indicate that Type 4 samples have largely involved fertile N-MORB source and do not appear to be as depleted as tholeiitic magmas formed at island arc settings (e.g. Peate et al. 1997). The lack of such depleted signatures and the relatively flat REE profiles suggest that a back-arc origin for Type 4 samples is more likely (e.g. Gribble et al. 1998). As mentioned above, the existence of N-MORB- and E-MORB-type melts are known from back-arc basins, thus, it might have been the case that Type 1 and 2 samples also formed at the same subduction zone system from which Type 4 samples have originated. Indeed, this idea is reinforced by the existence of these three distinct chemical types (N-MORB, E-MORB and BABB) from the same unit (i.e. the Daday Unit).

Type 3 samples possess OIB-like characteristics. Although such elemental signatures are typically found in oceanic islands (e.g. Sun and McDonough 1989; Chauvel et al. 1992), they can also be encountered at some continental rifts as well as at mid-ocean ridges and back-arc basins (e.g. Hickey-Vargas et al. 2006; Furman et al. 2006; Hoernle et al. 2011). However, the close geological association of Type 3 samples with the chemical types 1, 2 and 4 at several places of the Daday-Araç Transect (Fig. 3 and 6), which are of oceanic origin, may suggest that these OIB-like lithologies have similarly formed in a similar tectonic environment, namely an oceanic back-arc setting. The OIB-like melts are even isotopically more enriched than those of E-MORB-type magmas, suggesting that OIB-type magmas are relatively undiluted by melts of depleted peridotite.

Type 5 samples clearly exhibit oceanic affinities as evidenced by their highly depleted signatures. The depleted geochemical signatures are typical among magmas developed at island arcs, which is generally attributed to the melt extraction taking place in the back-arc region (e.g. Woodhead et al. 1998). Also, some Type 5 samples are somewhat unusual in that they display fractionated LREE-MREE profiles and depletion in moderately incompatible elements (Fig. 10). Such elemental profiles and the highly depleted nature of Type 5 samples seem to be similar to those of boninites (e.g. Cameron et al. 1983) (Fig. 11). Boninites are unusual volcanic rocks with intermediate SiO_2 and high MgO contents (e.g. Hickey and Frey 1982). However, since Type 5 samples have rather low SiO_2 contents, we prefer to use the term “boninitic” instead of “boninite” for these samples. The existence of boninitic melts is restricted to the intra-oceanic arcs and they generally appear to have been generated at the initiation of arc magmatism (e.g. Pearce et al. 1994). The LREE-enriched character of some boninitic magmas have been linked to the involvement of OIB-type component or fluids and/or melts derived from subducting oceanic lithosphere (e.g. Cameron et al. 1983; Kostopoulos and Murton 1992).

GEODYNAMIC CONSTRAINTS

The mafic lithologies from the Daday, Saka and Domuz Dağ units display an extensive geochemical variation (Figs. 10, 12 and 13) and they are characterized by different metamorphic grades. Thus, it may first seem that the protoliths of these metamorphic rocks have formed at diverse tectonic settings. However, as also mentioned at the beginning, the presence of distinct metamorphic styles does not mean that the origin of protoliths should also be different (e.g. Sayit and Göncüoğlu 2013). Also, the existence of diverse geochemical signatures does not necessarily mean that the samples should come from a number of tectonic settings. Back-arc basins, for example, are one such place where various chemical species can be found, including BABB-, IAB-, N-MORB-, E-MORB- and OIB-like signatures (e.g. Leat et al. 2000, 2004; Pearce et al. 2005; Hickey-Vargas et al. 2006). Combining these with the fact that the distinct chemical groups are in close association in the field (Fig. 2, 3 and 5) suggests that these units may have originated from an intra-oceanic arc-basin system. It is also noteworthy that the three metamorphic units comprise all chemical groups except for N-MORB-type, which is absent in the Saka and Domuz Dağ Units (Fig. 14). However, this chemical type (Type 1) is only represented by a single sample and the lack of this signature in the latter units may be due to sampling bias. Also, as mentioned before, this sample has not been directly recovered from the Daday Unit itself, but it occurs as a mélange block within the Arkot Dağ Mélange. Thus, apart from their formation at similar tectonic settings (i.e. intra-oceanic arc-basin system), the variety and distribution of geochemical signatures also appear to be similar. This suggests the possibility that the low-grade Daday Unit and high-grade Domuz Dağ Unit may, in fact, have originated from the same arc-basin system.

Another important point is that the mafic lithologies from the Ayli Dağ Ophiolite and Arkot Dağ Mélange, in general, share similar characteristics with those from the Daday, Saka and Domuz Dağ units, suggesting a genetic link between them.

The age of the protoliths of the mafic rocks from these metamorphic units is poorly constrained. However, a Middle Jurassic minimum depositional age has been proposed for the metasediments of the Martin Group of Okay et al (2013), which is the equivalent of the Daday Unit in our study. Our recent work on the age of detrital zircons from quartzites of the Daday Unit (Göncüoğlu et al. in prep), however, suggests that the maximum deposition age of the unit is Middle Triassic.

The mafic rocks of the Ayli Dağ Ophiolite exhibit predominant BABB-type characteristics with minor island arc signatures (Göncüoğlu et al. 2012). Similarly, the mafic lithologies from Arkot Dağ Mélange to the southwest of Kastamonu display similar geochemical characteristic, with BABB-type signatures being the common one (Göncüoğlu et al. 2014). As discussed above, BABB- and island arc-type characteristic are also observed in the Daday and Domuz Dağ units. We must also note that the Daday-type metamorphics with BABB-type signatures are also found as blocks within the Arkot Dağ Mélange as revealed by the present study. Other geochemical signatures (i.e. N-MORB, E-MORB, and OIB) have not been found yet from the Ayli Dağ Ophiolite. E-MORB- and OIB-type signatures are also not encountered in the Arkot Dağ Mélange. N-MORB-like signatures, however, have been reported from a huge slide block within the Arkot Dağ Mélange to the east of Bolu (Göncüoğlu et al. 2008). In addition, the N-MORB-type metabasic sample from the present study represents a Daday-type block within the Arkot Dağ Mélange, thus indicating that N-MORB-type lithologies are not uncommon.

The geochemical character of the Ayli Dağ Ophiolite strongly argues for its generation above an intra-oceanic arc-basin system (Göncüoğlu et al. 2012). The radiolarian cherts overlying pillow basalts have yielded an age of Middle Jurassic (Göncüoğlu et al. 2012).

This is the oldest age obtained thus far from the IPS zone and clearly implies that there was an ongoing subduction within the IPO during the Middle Jurassic. The data acquired from the basaltic slide blocks of the Arkot Dağ Mélange seem to be consistent with results above. The geochemical signatures of the mafic blocks and their geological characteristics call for the presence of an oceanic environment. The silicified mudstone interlayered with the N-MORB-type basalts has yielded an age of Late Jurassic (Göncüoğlu et al. 2008). Although it is difficult to say whether these N-MORB-type magmas were produced on a mid-ocean ridge or a back-arc basin, they have clearly been a part of an oceanic spreading environment. However, considering the younger age (Late Jurassic) of the N-MORB-type basalts, it is possible that these basalts may represent relatively evolved stage of the back-arc spreading represented by the Ayli Dağ Ophiolite. Whether the Late Jurassic basalts are closely connected to the arc-basin system or not, they obviously indicate that the IPO basin was still open during the Late Jurassic.

Our data suggest that the mafic rocks from Daday and Domuz Dağ units reflect a similar origin (i.e. oceanic arc-basin system) to the mafic rocks from the Ayli Dağ Ophiolite and Arkot Dağ Mélange (Göncüoğlu et al. 2008, 2012, 2014). As noted before, however, the Daday and Domuz Dağ units also involve enriched geochemical characteristics (E-MORB and OIB). The absence of these signatures in the Ayli Dağ Ophiolite and Arkot Dağ Mélange may be due to the insufficient sampling. Alternatively, this may also be linked to the site of melt generation during the temporal development of the arc-basin system. The enriched mantle, for example, in the form of blobs of a mantle plume may be introduced to the area of back-arc basin via mantle flow entering from the sides (e.g. Leat et al. 2000). Thus, in this case, the segments close to the edges of the back-arc would be the most influenced, reflecting the E-MORB- to OIB-like signatures. Another mechanism would be preferential melting of the easily fusible, enriched lithologies by a process like slab roll-back, which allows fertile mantle to migrate into the source region. Alternatively, the occurrence of slab window or slab break-off developing in response to the detachment of the slabs may also introduce fertile asthenospheric mantle into the melting region and can cause the preferential melting of the enriched blobs within the depleted matrix (e.g. Hole et al. 1995).

The mafic rocks collected from the different tectonic units of the IPS zone are representative of the IPO basin, i.e. a wide oceanic area located between the IZ and SK continental microplates. Thus, an overall evaluation of the geochemical features of these mafic rocks suggests that the IPO basin has included necessarily a well-developed arc-basin system.

Whereas the Ayli Dağ Ophiolite can be regarded as an obducted slice of back-arc oceanic lithosphere, the Arkot Dağ Mélange is considered as the Late Cretaceous sedimentary deposits originated during the obduction (Göncüoğlu et al. 2014). In this picture, the Domuz Dağ and Daday units, both affected during the Late Jurassic (Marroni et al. 2014) to Early Cretaceous (Akbayram et al. 2012; Okay et al. 2013) by a metamorphic event ranging from low-grade blueschist to high-pressure amphibolite and eclogite facies, seems to be the result of the convergence-related processes, which led to the closure of the IPO basin. Even if they have been metamorphosed under different conditions, the common geochemical signatures of the mafic rocks preserved in the Daday and Domuz Dağ metamorphic units indicates that they have been derived from the same domain, namely an intra-oceanic arc-basin system.

These results seem to indicate that two alternative hypotheses can be proposed for the geodynamic reconstruction of the IPO basin. In the first hypothesis, the IPO basin included also an older oceanic crust, probably Triassic in age (e.g. Tekin et al. 2012), whose subduction opened a SSZ basin in the Middle Jurassic (Yilmaz 1990, Robertson and Ustaömer 2004; Akbayram et al. 2012; Göncüoğlu et al. 2014). The presence of an older (Triassic) ocean is supported by the presence of oceanic rocks now accreted in the Karakaya Complex (Sayit and Göncüoğlu 2013). Jurassic MOR-type basalts within the IPS (Göncüoğlu et al. 2008) suggest that the opening of the SSZ basin is contemporaneous with the active spreading in the Intra-Pontide Ocean. A subsequent, younger subduction of SSZ oceanic lithosphere is required in this hypothesis in order to explain the metamorphism of the mafic rocks detected in the Daday and Domuz Dağ units. The inception of the second subduction occurred in the Late Jurassic-Early Cretaceous time span when the continental margin of the Sakarya continent was submerged and covered by basinal deposits (Fig. 15).

In the second, alternative hypothesis, IPO basin can be considered as an arc-basin system and the subduction responsible of its opening was located southward of the SK microplate within the Izmir-Ankara branch of Neotethys. This second hypothesis is not preferred in this study, as it is not supported by reliable evidence. In contrast, the oldest SSZ-type oceanic crust, hence the initial intra-oceanic subduction in this branch is not older then mid Cretaceous in age (Göncüoğlu et al. 2010).

REGIONAL CORRELATIONS

As discussed above, the collected data as well as the available data present in literature (Şengör and Yılmaz 1981; Göncüoğlu et al. 1987; Yılmaz 1990; Göncüoğlu and Erendil 1990; Yılmaz et al. 1995, 1997; Okay and Tüysüz 1999; Elmas and Yiğitbaş 2001; Robertson and Ustaömer 2004; Okay et al. 1996, 2013; Göncüoğlu et al. 2008, 2014; Marroni et al. 2014) indicate that the IPS zone is characterized by the occurrence of Middle to Late Jurassic ophiolites as separate tectonic units, slide blocks within the Cretaceous ophiolitic mélanges or as metaophiolites of probable Jurassic age in the subduction-related mèlanges affected by the Late Jurassic-Early Cretaceous metamorphism. All the fragments recognized in the IPS zone have been derived from an oceanic basin above a supra-subduction zone in which the melts was sourced from the depleted asthenospheric mantle metasomatized during the subduction process.

These findings suggest that 1) the spreading was active along the IPO basin during the Middle to Late Jurassic time and 2) the subduction and related development of an accretionary wedge have existed from the Late Jurassic to Early Cretaceous time span.

In the eastern Mediterranean area, these features are not only restricted to the IPS zone; but also to the other ophiolites from the suture zones located at the edge of the Eurasia continental plate.

The Dinaric-Hellenic belt, for instance, is characterized by the ophiolites known as the Guevgueli Complex that has obducted over the Adria-Pelagonian continental margin (Bébien 1983; Bébien et al. 1986; 1987; Saccani et al. 2008; Bortolotti et al. 2013). These ophiolites of Middle to Late Jurassic ages (Kukoč et al. 2014) are characterized by ophiolite sequences including only volcanic and subvolcanic rocks generated in a back-arc setting (Bébien et al. 1986, 1987; Saccani et al. 2008). The Guevgueli ophiolites are overlain by the metamorphic units of the Rhodope massif, where eclogites, amphibolites, gneisses and marbles have been affected by high-pressure metamorphism of Late Jurassic-Early Cretaceous age (e.g Burg, 2012). The back-arc ophiolites as well as the associated metamorphic rocks can be traced from the southern Greece into Sporades islands located in the Aegean Sea, about 200 km west of the outcrops on land of the IPS zone in the western Turkey.

To the southeast, the SSZ-type ophiolites of Early Jurassic age have been reported in the NE Turkey as the Refahiye ophiolites (Ustaömer and Robertson 2010: Topuz et al. 2013; Robertson et al. 2014). These ophiolites are located within the Izmir-Ankara-Erzincan suture zone between the Pontides and the Menderes-Taurus terranes. By this they are unrelated to the IPS. They are underlain by a Late Cretaceous mélange and tectonically associated with the metamorphic rocks of Early to Middle Jurassic age, consisting of marbles, serpentinites, phyllites but also by amphibolites, garnet-bearing amphibolites, garnet-bearing micaschists and eclogites.

Similar geological features have been found in the Armenian ophiolites (Sevan, Stepanavan and Vedi ophiolites) that crop out eastward of the Izmir-Ankara-Erzincan suture zone, which has formed in a similar tectonic setting (Galoyan et al. 2009; Rolland et al. 2010; Hässig et al. 2014). The data provided by Galoyan et al. (2009) and Hässig et al. (2014) suggest these ophiolites to have been developed in a Early Jurassic back-arc basin. These ophiolites have been emplaced by a top-to-the-south obduction on the continental margin of the South Armenian plate during the Coniacian time. The Armenian ophiolites are associated with the Amassia–Stepanavan blueschist-ophiolite complex of the Lesser Caucasus (Rolland et al. 2010). This complex, which includes calcschists, metaconglomerates, quartzites, gneisses and metabasites, has been interpreted as a tectonic mèlange affected by blueschist metamorphism within an accretionary prism during the Cenomanian–Turonian times (Rolland et al. 2010).

The overall picture arising from the Dinaric-Hellenic belt as well as from the IPS zone indicates that an intra-oceanic back-arc basin have existed during the Jurassic time within the IPS between the Sakarya Composite Terrane and the southern edge of the Eurasian plate (e.g. Marroni et al. 2014). Towards east the co-eval intra-oceanic subduction within the Izmir-Ankara-Erzincan Ocean created another back-arc basin between the Menderes-Tauride block and the southern margin of the Eurasian plate (e.g. Robertson et al. 2014). Both basins probably formed as a result of north-dipping intra-oceanic subductions developed in the frame of the episodic accretion of different Gondwanan continental fragments (Istanbul-Zonguldak Terrane during the Late Paleozoic, basement of the Sakarya Terrane at the end of Triassic, Sakarya Composite Terrane in the west and Menderes-Tauride block in the East at Late Cretaceous) to the Eurasian plate during the Late Paleozoic to Late Cretaceous (e.g. Bortolotti and Principi 2005 and Topuz et al. 2014). The closure of the alpine back-arc basins was thus achieved by development of subduction accretionary prisms leading to high-pressure metamorphic belt of Late Jurassic–Early Cretaceous age running parallel to the continental margin of Eurasia. The diachronous closure of these back-arc basins from northwest to southeast (see discussion in Bortolotti et al. 2013; Rolland et al. 2010; Topuz et al. 2013) requires that the width of this back-arc basin increased towards the southeast.

CONCLUSIONS

The mafic rocks collected from the Arkot Dağ Mélange as well as from the Domuz Dağ, Saka and Daday units along two transects of the IPS zone in Northern Turkey display not only different metamorphism, but also exhibit extensive geochemical variation ranging from IAT, BABB and N-MORB to E-MORB and OIB. Despite this wide spectrum of geochemical signatures, all the analysed mafic rocks can be regarded to have originated from an intra-oceanic arc-basin system. This picture is confirmed by the available geochemical data from the Ayli Dağ Ophiolite (Göncüoğlu et al. 2012), Arkot Dağ Mélange (Göncüoğlu et al. 2008; 2014) and from the mafic/intermediate rocks of the andesite-bearing turbidites (Rice at al. 2006).

On the whole, it is possible to state that in the IPS zone several fragments of an arc-basin system are preserved, whose initiation occurred well before the Middle Jurassic. The new data from the IPZ zone with integration of the regional data from the Balkans and the Eastern Aegean points to existence of a wide intra-oceanic arc-basin system running parallel to the edge of the Eurasian plate during the Jurassic time. This arc-basin system was the result of a northward-dipping subduction developed in the frame of the episodic accretion of Gondwana continental fragments to Eurasia plate. This hypothesis can provide new insights for the reconstruction of the tectonic history of the IPO in the frame of the Mesozoic geodynamic evolution of the Eastern Mediterranean.

ACKNOWLEDGEMENTS

The authors gratefully acknowledge Yann Rolland and two anomynous reviewers. The research has been funded by Darius Project (resp. M. Marroni). This research benefits also by grants from PRIN 2008 and PRIN 2010-11 project (resp. M. Marroni) and from IGG-CNR.

REFERENCES

Akbayram K, Okay AI, Satır M (2012) Early Cretaceous closure of the Intra-Pontide Ocean in western Pontides (northwestern Turkey). J Geodyn. 65: 38-55

Allegre CJ, Turcotte DL (1986) Implications of a 2-Component Marble-Cake Mantle. Nature 323: 123-127

Bébien J. (1983) L'association ignée de Guevgueli. Ofioliti 8: 293-302

Bébien J, Dubois R, Gauthier A (1986) Example of ensialic ophiolites emplaced in a wrench zone; innermost Hellenic ophiolite belt (Greek Macedonia). Geology 14: 1016-1019

Bébien J, Baroz F, Capedri S, Venturelli G (1987) Magmatisme basiques associes a l'ouverture d'un bassin marginal dans les Hellenides Internes au Jurassique. Ofioliti 12: 53-70

Bedard JH (1999.) Petrogenesis of Boninites from the Betts Cove Ophiolite, Newfoundland, Canada: Identification of Subducted Source Components. J Petrol 40, 1853-1889

Bortolotti V, Chiari M, Marroni M, Pandolfi L, Principi G, Saccani E (2013) Geodynamic evolution of the ophiolites from Albania and Greece (Dinaric-Hellenic belt): one, two or more oceanic basins? Int J Earth Sci 102: 738-811

Bortolotti V, Principi G (2005) Tethyan ophiolites and Pangea break-up. Isl Arc 14:442–470

Burg J (2012) Rhodope: From Mesozoic convergence to Cenozoic extension. Review of petro-structural data in the geochronological frame. In: Skourtsos E, Lister GS (eds) The Geology of Greece. Journal of the Virtual Explorer Electronic Edition vol 42: paper 1

Cameron WE, Culloch MT, Walker DA (1983) Boninite Petrogenesis: chemical and Nd-Sr isotopic constraints. Earth Planet Sci Lett 65: 75-89

Catanzariti R, Ellero A, Göncüoğlu MC, Marroni M, Ottria G, Pandolfi L (2013) The Taraklı Flysch in the Boyalı area (Sakarya Terrane, Northern Turkey): Implications for the tectonic history of the Intrapontide Suture Zone. C R Geosci 345(11-12): 454-461

Chauvel C, Hemond C (2000) Melting of a complete section of recycled oceanic crust: Trace element and Pb isotopic evidence from Iceland. Geoch Geoph Geosys 1(1001) doi: 10.1029/1999GC000002

Chauvel C, Hofmann AW, Vidal P (1992) HIMU-EM: The French Polynesian connection. Earth Planet Sci Lett 110: 99-119

Class C, Miller DM, Goldstein S, Langmuir C (2000) Distinguishing melt and fluid subduction components in Umnak Volcanics, Aleutian Arc. Geoch Geoph Geosyst 1, paper 1999GC000010.

Condie K (2005) High field strength element ratios in Archean basalts: a window to evolving sources of mantle plumes? Lithos 79: 491-504

Ellero A, Ottria G, Marroni M, Pandolfi L, Göncüoğlu MC (2015) Analysis of the North Anatolian Shear Zone in Central Pontides (northern Turkey): Insight for geometries and kinematics of deformation structures in a transpressional zone. J Struct. Geol doi:10.1016/j.jsg.2014.12.003

Elmas A, Yiğitbaş E (2001) Ophiolite emplacement by strike-slip tectonics between the Pontide Zone and the Sakarya Zone in northwestern Anatolia, Turkey. Int J Earth Sci 90: 257-269

Furman T, Kaleta KM, Bryce JG, Hanan BB (2006) Tertiary mafic lavas of Turkana, Kenya: Constraints on East African Plume structure and the occurrence of high-μ volcanism in Africa. J Petrol 47: 1221-1244

Galoyan G, Rolland Y, Sosson M, Corsini M, Billo S, Verati C, Melkonyan R (2009) Geology, geochemistry and 40Ar/39Ar dating of Sevan ophiolites (Lesser Caucasus, Armenia): evidence for Jurassic Back-arc opening and hot spot event between the South Armenian Block and Eurasia. J Asian Earth Sci 34: 135-153.

Göncüoğlu MC, Erendil M (1990) Pre-Late Cretaceous tectonic units of the Armutlu Peninsula. Proc of 8th Turkish Petroleum Congress 8: 161-168

Göncüoğlu MC, Dirik K, Kozlu H (1997) Pre-Alpine and Alpine Terranes in Turkey: explanatory notes to the terrane map of Turkey. Ann Geol Pays Hellen 37: 515-536

Göncüoğlu MC, Sayit K, Tekin UK (2010) Oceanization of the northern Neotethys: Geochemical evidence from ophiolitic mélange basalts within the Izmir-Ankara suture belt, NW Turkey. Lithos,116: 175-187

Göncüoğlu MC, Marroni M, Sayit K, Tekin UK, Ottria G, Pandolfi L, Ellero A (2012) The Aylı Dağ ophiolite sequence (central-northern Turkey): A fragment of Middle Jurassic oceanic lithosphere within the Intra-Pontide suture zone. Ofioliti 37: 77-91

Göncüoğlu MC, Marroni M, Pandolfi L, Ellero A, Ottria G, Catanzariti R, Tekin UK, Sayit K (2014) The Arkot Dağ Mélange in Araç area, central Turkey: Evidence of its origin within the geodynamic evolution of the Intra-Pontide suture zone. J Asian Earth Sci 85: 117-139

Göncüoğlu MC, Turhan N, Senturk K, Ozcan A, Uysal S (2000) A geotraverse across NW Turkey: tectonic units of the Central Sakarya region and their tectonic evolution. In: Bozkurt E, Winchester J, Piper JA (eds.) Tectonics and magmatism in Turkey and the surrounding area. Geological Society of London Special Publication vol 173, pp 139-161.

Göncüoğlu MC, Erendil M, Tekeli O, Aksay A, Kuscu A, Urgun B (1987) Geology of the Armutlu Peninsula. IGCP-5 Guide Book 5: 12-18

Göncüoğlu MC, Gürsu S, Tekin UK, Koksal S (2008) New data on the evolution of the Neotethyan oceanic branches in Turkey: Late Jurassic ridge spreading in the Intra-Pontide branch. Ofioliti 33: 153-164

Görür N, Monod O, Okay AI, Şengör AMC, Tüysüz O, Yiğitbaş E, Sakinc M, Akkök R (1997) Palaeogeographic and tectonic position of the Carboniferous rocks of the western Pontides (Turkey) in the frame of the Variscan belt. Bull Soc Géol France 168: 197–205

Green TH (1995) Significance of Nb/Ta as an indicator of geochemical processes in the crust-mantle system. Chemical Geology 120, 347-359

Gribble RF, Stern RJ, Newman S, Bloomer SH, O'Hearn T (1998) Chemical and isotopic composition of lavas from the Northern Mariana Trough: Implications for magma genesis in back-arc basins. J Petrol 39: 125-154

Haase KM, Devey CW (1994) The petrology and geochemistry of Vesteris Seamount, Greenland Basin – an intraplate alkaline volcano of non-plume origin. J Petrol 35: 295-328

Hässig M, Rolland Y, Sosson M, Galoyan G, Sahakyan L, Topuz G, Çelik OF, Avagyan, A, Müller C (2014) Linking the NE Anatolian and Lesser Caucasus ophiolites: evidence for large-scale obduction of oceanic crust and implications for the formation of the Lesser Caucasus-Pontides Arc. Geod Acta, 26 (3-4): 311-330

Hickey RL, Frey FF (1982) Geochemical chAraçteristics of boninite series volcanics: implications for their source. Geoch Cosmoch Acta 46: 2099-2115

Hickey-Vargas R, Savov I, Bizimis M, Ishii T, Fujioka K (2006) Origin of diverse geochemical signatures in igneous rocks from the West Philippine Basin: Implications for tectonic models, In: Christie D (ed) Back-Arc Spreading Systems: Geological, Biological, Chemical and Physical Interactions. AGU Geophysical Monograph Series vol 166, pp 287-303

Hoernle K, Folkmar H, Kokfelt TF, Haase K, Garbe-Schönberg, Werner R (2011) On- and off-axis chemical heterogeneities along the South Atlantic Mid-Ocean-Ridge (5-11° S). Earth Planet Sci Lett 306: 86-97

Hofmann AW, White WM (1982) Mantle plumes from ancient oceanic crust. Earth Planet Sci Lett 57: 421-436

Hole MJ, Saunders AD, Rogers G, Sykes MA (1995) The relationship between alkaline magmatism, lithospheric extension and slab window formation along continental destructive plate margins. In: Smellie JL (ed) Volcanism associated with extension at consuming plate margins. Geological Society Special Publications vol 81, pp 265-285

John T, Scherer EE, Haase K, Schenk V (2004) Trace element fractionation during fluid-induced eclogitization in a subducting slab: trace element and Lu–Hf–Sm–Nd isotope systematics. Earth Planet Sci Lett 227: 441–456.

Kukoc D, Gorican S, Košir A, Belak M, Halamic J,· Hrvatovic H (2014) Middle Jurassic age of basalts and the post- obduction sedimentary sequence in the Guevgueli Ophiolite Complex (Republic of Macedonia). Int J Earth Sci 104: 425-447

Kostopoulos DK, Murton BJ (1992) Origin and distribution of components in boninite genesis: significance of the OIB component. In: Parson LM, Murton BJ, Browning P (eds) Ophiolites and their Modern Oceanic Analogues. Geological Society Special Publications vol 60, pp 133-154

Ito G, Mahoney JJ (2005) Flow and melting of a heterogeneous mantle: 1. Method and importance to the geochemistry of ocean island and mid-ocean ridge basalts. Earth Planet Sci Lett 230: 29-46

Leat PT, Livermore RA, Millar IL, Pearce JA (2000) Magma supply in back-arc spreading centre segment E2, East Scotia Ridge. J Petrol 41: 845-866

Leat PT, Pearce JA, Barker PF, Millar IL, Barry TL, Larter RD (2004) Magma genesis and mantle flow at a subducting slab edge: The South Sandwich arc-basin system, Earth Planet. Sci. Lett. 227: 17–35

Marroni M, Frassi C, Göncüoğlu MC, Di Vincenzo G, Pandolfi L, Rebay G, Ellero A, Ottria G (2014) Late Jurassic amphibolite-facies metamorphism in the Intra-Pontide Suture Zone (Turkey): an eastward extension of the Vardar Ocean from the Balkans into Anatolia? J Geol Soc 171: 605-609.

Niu YL, MJ O'Hara (2004) Mantle plumes are not from ancient oceanic crust. In: Hékinian R, Stoffers P (eds) Oceanic Hotspots. Springer-Verlag, New York, pp 239-252.

Niu Y, Bideau D, Hekinian R, Batiza R (2001) Mantle compositional control on the extent of mantle melting, crust production, gravity anomaly, ridge morphology, and ridge segmentation: a case study at the Mid-Atlantic Ridge 33-35°. Earth Planet Sci Lett 186: 383-399

Niu Y, Collerson KD, Batiza R, Wendt JI, Regelous M (1999) Origin of enriched-type mid-ocean rigde basalt at ridges far from mantle plumes: The East Pacific Rise at 11°20'N. J Geoph Res 104: 7067-7087

Okay AI, Göncüoğlu MC (2004) The Karakaya Complex: A review of data and concepts. Turkish J Earth Sci 13: 77-95

Okay AI, Satır M, Siebel W (2006) Pre-Alpide Palaeozoic and Mesozoic orogenic events in the Eastern Mediterranean region. In: Gee DG, Stepherson RA (eds) European Lithosphere Dynamics. Geological Society Special Publications vol. 32, pp. 389–406.

Okay AI, Tüysüz O (1999) Tethyan sutures of northern Turkey. In: Durand B, Olivet JL, Horvath E, Serrane M (eds.) The Mediterranean basins, extension within the Alpine Orogen. Turkish J Earth Sci 156: 475-515.

Okay AI, Whitney DL (2010) Blueschists, eclogites, ophiolites and suture zones in northwest Turkey: A review and a field excursion guide. Ofioliti 35: 131-172

Okay AI, Satır M, Maluski H, Siyako M, Monié P. Metzger R, Akyüz S (1996) Palaeo- and Neo-Tethyan events in northwest Turkey. In: Yin E, Harrison M (eds) Tectonics of Asia. Cambridge University Press, Cambridge: 420–441

Okay AI, Sunal G, Sherlock S, Altiner D, Tüysüz O, Kylander-Clark ARC, Aygül M (2013) Early Cretaceous sedimentation and orogeny on the active margin of Eurasia: Southern Central Pontides, Turkey. Tectonics 32: 1247-1271

Okay AI (2000) Was the Late Triassic orogeny in Turkey caused by the collision of an oceanic plateau? In: Bozkurt E, Winchester JA, Piper JDA (eds) Tectonic and magmatism in Turkey and surrounding area. Geological Society Special Publications vol 173, pp 25–41

Pearce JA (1983) The role of sub-continental lithosphere in magma genesis at active continental margins. In: Hawkesworth CJ, Norry MJ (eds.) Continental basalts and mantle xenoliths. Shiva Publications pp 230-249

Pearce JA, Peate DW (1995) Tectonic implications of the composition of volcanic arc magmas. Annual Rev Earth Planet Sci 23: 251-285

Pearce JA, Stern RJ (2006) Origin of back-arc basin magmas: Trace element and isotope perspectives. In: Christie D (ed) Back-Arc Spreading Systems: Geological, Biological, Chemical and Physical Interactions, AGU Geophysical Monograph Series vol 166, pp 63-86

Pearce JA, Baker PE, Harvey PK, Luff IW (1995) Geochemical evidence for subduction fluxes, mantle melting and fractional crystallization beneath the South Sandwich Island Arc. J Petrol 36: 1073-1109

Pearce JA, Ernewein M, Bloomer SH, Parson LM, Morton BJ, Johnson LE (1994) Geochemistry of Lau Basin volcanic rocks: influence of ridge segmentation and arc proximity. In: Smellie JL (ed) Volcanism Associated with Extension at Consuming Plate Margins. Geological Society Special Publications vol 81, pp 53-75.

Pearce JA, Stern JA, Bloomer SH, Fryer P (2005) Geochemical mapping of the Mariana arc-basin system: Implications for the nature and distribution of subduction components. Geoch Geoph Geosyst doi:10.1029/2004GC000895

Peate DW, Pearce JA, Hawkesworth CJ, Colley H, Edwards CMH, Hirose K (1997) Geochemical variations in Vanuatu arc lavas: the role of subducted material and a variable mantle wedge composition. J Petrol 38: 1331-1358

Rice SP, Robertson AHF, Ustaömer T (2006) Late Cretaceous-Early Cenozoic tectonic evolution of the Eurasian active margin in the Central and Eastern Pontides, northern Turkey. In: Robertson AHF (ed) Tectonic Development of the Eastern Mediterranean Region. Geological Society Special Publications vol 260, pp 413-445

Robertson AHF, Ustaömer T (2004) Tectonic evolution of the Intra-Pontide suture zone in the Armutlu Peninsula, NW Turkey. Tectonophysics 381: 175-209

Robertson AHF, Ustaömer T (2011) Role of tectonic-sedimentary mélange and Permian–Triassic cover units, central southern Turkey in Tethyan continental margin evolution. J Asian Earth Sci 40: 98-120

Robertson AHF, Ustaömer T (2012) Ion Probe U-Pb dating of the Central Sakarya Basement: a peri-Gondwana terrane intruded by Late Lower Carboniferous subduction/collision-related granitic rocks. Turk J Earth Sc 21: 961-1007

Robertson AHF, Parlak O, Ustaömer T, Taslı K, Inan N, Dumitrica P, Karaoğlan F (2014) Subduction, ophiolite genesis and collision history of Tethys adjacent to the Eurasian continental margin: new evidence from the Eastern Pontides, Turkey. Geodin Acta, doi: 10.1080/09853111.2013.877240

Rolland Y, Galoyan G, Sosson M, Melkonian R Avagyan A (2010) The Armenian ophiolites: insights for Jurassic back-arc formation, Lower Cretaceous hot-spot magmatism, and Upper Cretaceous obduction over the South Armenian Block. Geological Society Special Publications vol 340, pp 353-382.

Saccani E, Padoa E, Photiades A (2003) Triassic mid-ocean ridge basalts from the Argolis Peninsula (Greece): new constraints for the early oceanization phases of the Neo-Tethyan Pindos basin. In: Dilek Y, Robinson PT (eds) Ophiolites in Earth History. Geological Society Special Publications vol 218, pp 109-127

Saccani E, Bortolotti V, Marroni M, Pandolfi L, Photiades A, Principi G (2008) The Jurassic association of backarc basin ophiolites and calc-alkaline volcanics in the Guevgueli Complex (Northern Greece): implication for the evolution of the Vardar Zone, Ofioliti 33: 209-227.

Sayit K (2013) Immobile trace element systematics of oceanic island basalts: the role of oceanic lithosphere in creating the geochemical diversity. Ofioliti 38: 101-120

Sayit K, Göncüoğlu MC (2013) Geodynamic evolution of the Karakaya Melange Complex, Turkey: A review of geological and petrological constraints. J Geodyn 65: 56– 65

Sayit K, Göncüoğlu MC, Furman T (2010) Petrological reconstruction of Triassic seamounts/oceanic islands within the Palaeotethys: Geochemical implications from the Karakaya subduction/accretion Complex, Northern Turkey. Lithos 119: 501-511

Şengör AMC, Yılmaz Y, Ketin İ (1980) Remnants of a pre-Late Jurassic ocean in northern Turkey: fragments of Permian-Triassic Paleo-Tethys. Geol Soc Am Bull 91: 599–609

Şengör AMC, Yılmaz Y (1981) Tethyan evolution of Turkey: a plate tectonic approach. Tectonophysics 75: 181-241

Şengör AMC, Tüysüz O, Imren C, Sakinc M, Eyidogan H, Görür N, Le Pichon X, Rangin C (2005) The North Anatolian Fault: A New Look. Annual Rev Earth Planet Sci 33: 37-112

Spandler C, Hermann J, Arculus R, Mavrogenes J (2004) Geochemical heterogeneity and element mobility in deeply subducted oceanic crust: insights from high-pressure mafic rocks from New Caledonia. Chem Geol 206: 21-42

Staudigel H, Plank T, White B, Schmincke H-U (1996) Geochemical fluxes during seafloor alteration of the basaltic upper oceanic crust: DSDP sites 417 and 418. Geoph Mon Series 96: 19-38.

Sun S-S, McDonough WF (1989) Chemical and isotopic systematics of oceanic basalts: implications for mantle composition and processes. In: A.D. Saunders and M.J. Norry (Eds.), Magmatism in the ocean basins. Geological Society Special Publications vol 42, pp 313-345

Tatsumi Y, Eggins S, (1995) Subduction Zone Magmatism. Blackwell, pp 211

Tekeli O (1981) Subduction complex of pre-Jurassic age, northern Anatolia, Turkey. Geology 9: 68-72

Tekin UK, Göncüoğlu MC, Pandolfi L, Marroni M (2012) Middle-Late Trias radiolarian cherts from the Arkotdağ mélange in northern Turkey: implications for the life span of the northern Neotethyan branch. Geod Acta 25: 305-319

Topuz G, Göçmengil G, Rolland Y, Çelik ÖF, Zack T, Schmitt AK (2013) Jurassic accretionary complex and ophiolite from northeast Turkey: No evidence for the Cimmerian continent. Geology 41: 255-258

Topuz G, Çelık ÖF, Şengör AMC, Altintaş İE, Zack T, Rolland Y, Barth M (2014) Jurassic ophiolite formation and emplacement as backstop to a subduction-accretion complex in northeast Turkey, the Refahıye ophiolite, and relation to the Balkan ophiolites. Am J Sci 31310, 1054-1087

Tüysüz O (1990) Tectonic evolution of a part of the Tethyside Orogenic Collage: the Kargı Massif, Northern Turkey. Tectonics 9: 141-160

Ustaömer T, Robertson AHF (1993) A Late Paleozoic-Early Mesozoic marginal basin along the active southern continental margin of Eurasia: Evidence from the Central Pontides (Turkey) and adjacent regions. Geol J 28: 219-238

Ustaömer T, Robertson AHF (1999) Geochemical evidence used to test alternative plate tectonic models for pre-Upper Jurassic (Palaeotethyan) units in the Central Pontides, N Turkey. Geol J 34: 25-53

Ustaömer T, Robertson AHF (2010) Late Palaeozoic-Early Cenozoic tectonic development of the Eastern Pontides (Artvin area), Turkey: stages of closure of Tethys along the southern margin of Eurasia. In: Sosson M, Kaymakçı N, Stephenson RA, Bergerat F, Starostenko V (eds.) Sedimentary Basin Tectonics from the Black Sea and Caucasus to the Arabian Platform. Geological Society Special Publications 340, 281-327

Workman RK, Hart SR (2005) Major and trace element composition of the depleted MORB mantle (DMM). Earth Planet Sci Lett 231: 53-72

Woodhead JD, Eggins SM, Johnson RW (1998) Magma genesis in the New Britain island arc: further insights into melting and mass transfer processes. J Petrol 39: 1641-1668

Yiğitbaş E, Elmas A, Yılmaz Y (1999) Pre-Cenozoic tectonostratigraphic components of the Western Pontides and their geological evolution. Geol J 34: 55–74

Yilmaz Y, Genc SC, Yiğitbaş E, Bozcu M, Yilmaz K (1995) Geological evolution of the late Mesozoic continental margin of Northwestern Anatolia. Tectonophysics 243: 155-171

Yılmaz Y (1990) Allochthonous terranes in the Tethyan Middle East, Anatolia and surrounding regions. Philosophical Transaction Royal Society of London A 331: 611–624

Yılmaz Y, Tüysüz O, Yiğitbaş E, Genç SC, Şengör AMC (1997) Geology and tectonic evolution of the Pontides. In: Robinson, A.G. (Ed.), Regional and Petroleum geology of the Black Sea and surrounding region. Bull Am Ass Petrol Geol 68: 183– 226

Zindler A, Hart S (1986) Chemical Geodynamics. Annual Rev Earth Planet Sci 14: 493-571

FIGURE CAPTIONS

FIGURE 1. The major tectonic zones of Turkey separated by sutures (black lines). IZ: Istanbul-Zonguldak Terrane. SK: Sakarya Terrane. AT: Anatolide-Tauride Terrane. NAF: North Anatolian Fault. EAF: East Anatolian Fault. IPS: Intrapontide Suture. Da: Daday. Bo: Boyalı. Ka: Kastamonu. To: Tosya. In red, Neogene to Holocene active regional structures are indicated.

FIGURE 2. Tectonic sketch map of the Boyalı-Daday transect. See Fig. 1 for map location. Samples used for geochemical study are also showed. Additional samples have been collected few kilometers south-east outside the map (IPS-10-54: 41°01’56.82”N, 33°43’32.02”E; IPS-10-56: 41°02’28.18”N, 33°43’53.47”E; IPS-10-52: 41°00’40.86”N, 33°42’02.66”E)

FIGURE 3. Tectonic sketch map of the Tosya- Emirköy transect. See Fig. 1 for map location. Samples used for geochemical study are also showed. Additional samples have been collected few kilometers north-east outside the map (5-8-2012: 41°18’00.77”N, 34°16’08.43”E; IPS-13-05: 41°17’18.07”N, 34°13’25.70”E; 4-8-2012: 41°15’19.17”N, 34°21’33.87”E; 4-3-2012: 41°16’37.74”N, 34°22’42.40”E; 13-7-13-1: 41°17’11.91”N, 34°09’44.21”E).

FIGURE 4. Sketch of the stratigraphy of the tectonic units recognized along the Boyalı-Daday and Tosya-Emirköy transects and their relationships with the Sakarya zone, Istanbul- Zondulgak zone and the overlying Eocene deposits.

FIGURE 5. Geological cross- sections of the Boyalı-Daday and Tosya-Emirköy transects.

FIGURE 6. Metamafic rocks cropping out along the Boyali - Daday and Tosya - Emirköy transects. a) Glaucophane-bearing amphibolites from Domuz Dağ Unit; b) relationships between amphibolites (amph) and micaschists (m-sch) from Domuz Dağ Unit; c) amphibolites from Saka Unit; d) relationships between amphibolites (amph) with albite-rich levels (ab), and micaschists (m-sch) from Saka Unit; e) actinolite-bearing schists from Daday Unit; f) relationships between

actinolite-bearing schists (m-bas) and phyllites (phy) from Daday Unit. For the field photos of mafic rocks from Arkot Dağ Mèlange see Göncüoğlu et al (2014).

FIGURE 7. Sketch of the tectono-stratigraphic units of the Intra-Pontide suture zone.

FIGURE 8. Plots of selected trace elements vs Zr.

FIGURE 9. Trace element and REE patterns of the metamorphic samples. Normalization values from Sun and McDonough (1989).

FIGURE 10. Chemical classification of the metamorphic rocks examined in this study on the basis of immobile element ratios (based on the diagram of Winchester and Floyd 1977 modified by Pearce 1996).

FIGURE 11. Zr/Y-Nb/Y and Nb/Yb-Th/Yb plots. Mariana Back-arc data from Pearce et al. (2005), South Sandwich Arc data from Pearce et al. (1995), Mid-Atlantic Ridge data from Niu et al. (2001). Average N-MORB, E-MORB and OIB values from Sun and McDonough (1989).

FIGURE 12. Plots of MORB-normalized Zr value against Zr/Nb and La/Sm. Data sources for Mariana Back-arc and South Sandwich Island Arc are the same as in Fig. 7. Miscellaneous boninite data from Cameron et al. (1983). Betts Cove boninites from Bedard (1999).

FIGURE 13. Geochemical modelling of the studied samples. E-DMM and DMM compositions of Workman and Hart (2004) have been adopted for the garnet and spinel peridotite sources, respectively. a) Garnet peridotite source is assumed to have the mode of 0.600 Ol+0.210 Opx+0.120 Cpx+0.070 Grt, which melts in the proportions 0.010 Ol+0.040 Opx+0.500 cpx+0.450 Grt. Spinel peridotite source has the mode of 0.565 Ol+0.220 Opx+0.180 Cpx+0.035 Spi and melts in the proportions of 0.200 Ol+0.150 Opx+0.550 Cpx+0.100 Spi. Both melting curves have been modelled according to batch melting. Straight lines represent melt-mixing lines between various degrees of Grt-facies melts (2%-9%) and 4.5% Spi-

facies melt. Melt fractions contributed by these facies were indicated by dots drawn at each 10% interval. b) The spinel peridotite curve has been calculated based on the same assumptions as in the first melting scheme. In constructing the second curve, however, first 25% batch melt is extracted from the spinel peridotite source and the residue is modified by 1% garnet-facies melt. This metasomatized source is assumed to have a mode of 0.700 Ol+0.220 Opx+0.065 Cpx+0.015 Spi, which melts in a fractional fashion with the proportions of 0.20 Ol+0.15 Opx+0.55 Cpx+0.10 Spi.

FIGURE 14. Comparison of trace element patterns of the mafic metamorphic rocks from Daday, Saka, Domuz Dağ and Arkot Dağ units.

FIGURE 15. Geodynamic reconstruction of the Intra-Pontide oceanic domain during the Jurassic and Early Cretaceous. See text for further explanations.

TABLE 1. Correlation chart among the different units of the study area. The correlation is based on both metamorphic/lithological features and location in the geological maps.

TABLE 2 Geochemical data of the studied mafic rocks.

Figure 1
Click here to download Figure: Fig1.eps

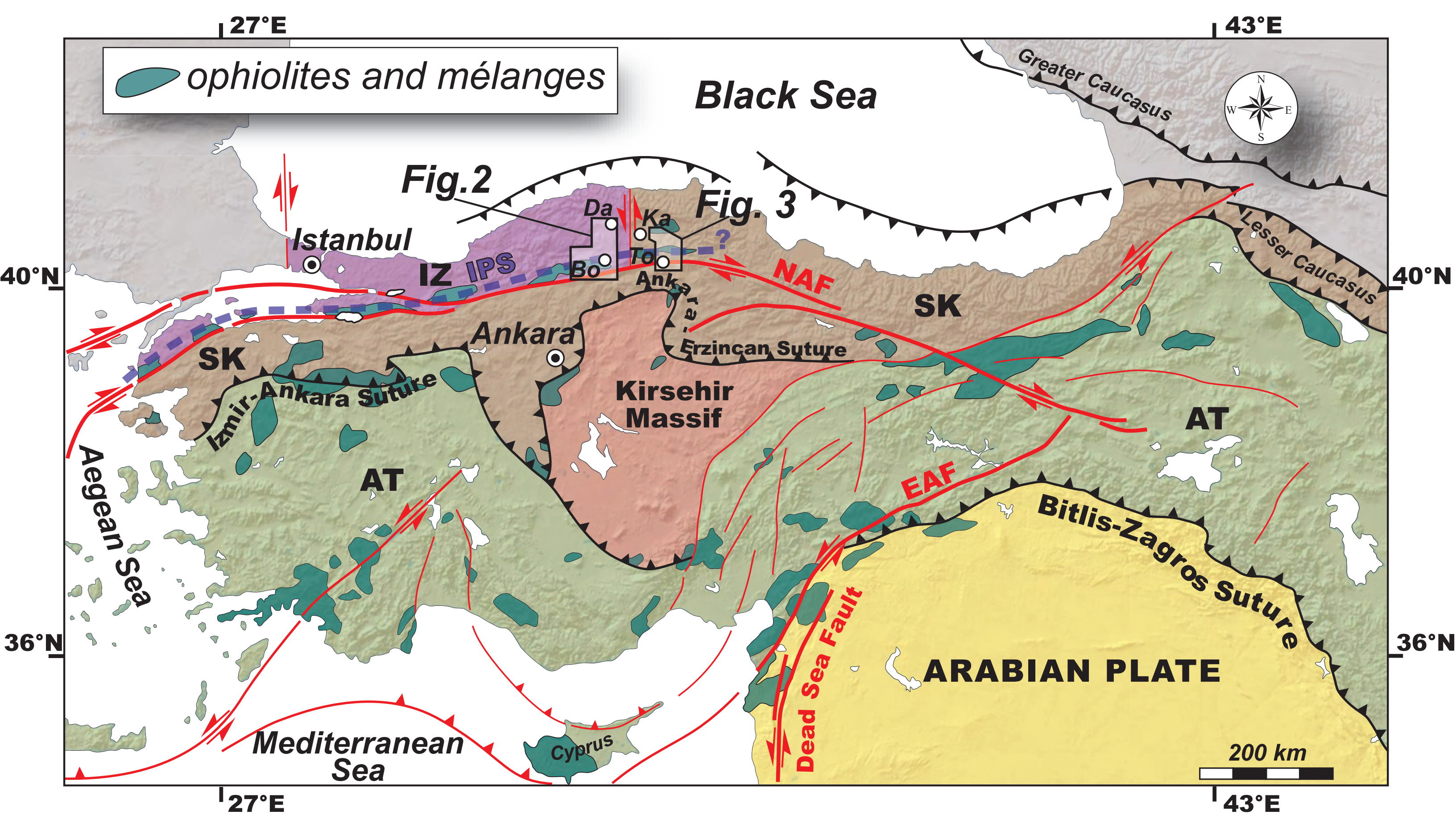

Figure 2
Click here to download Figure: Fig2.eps

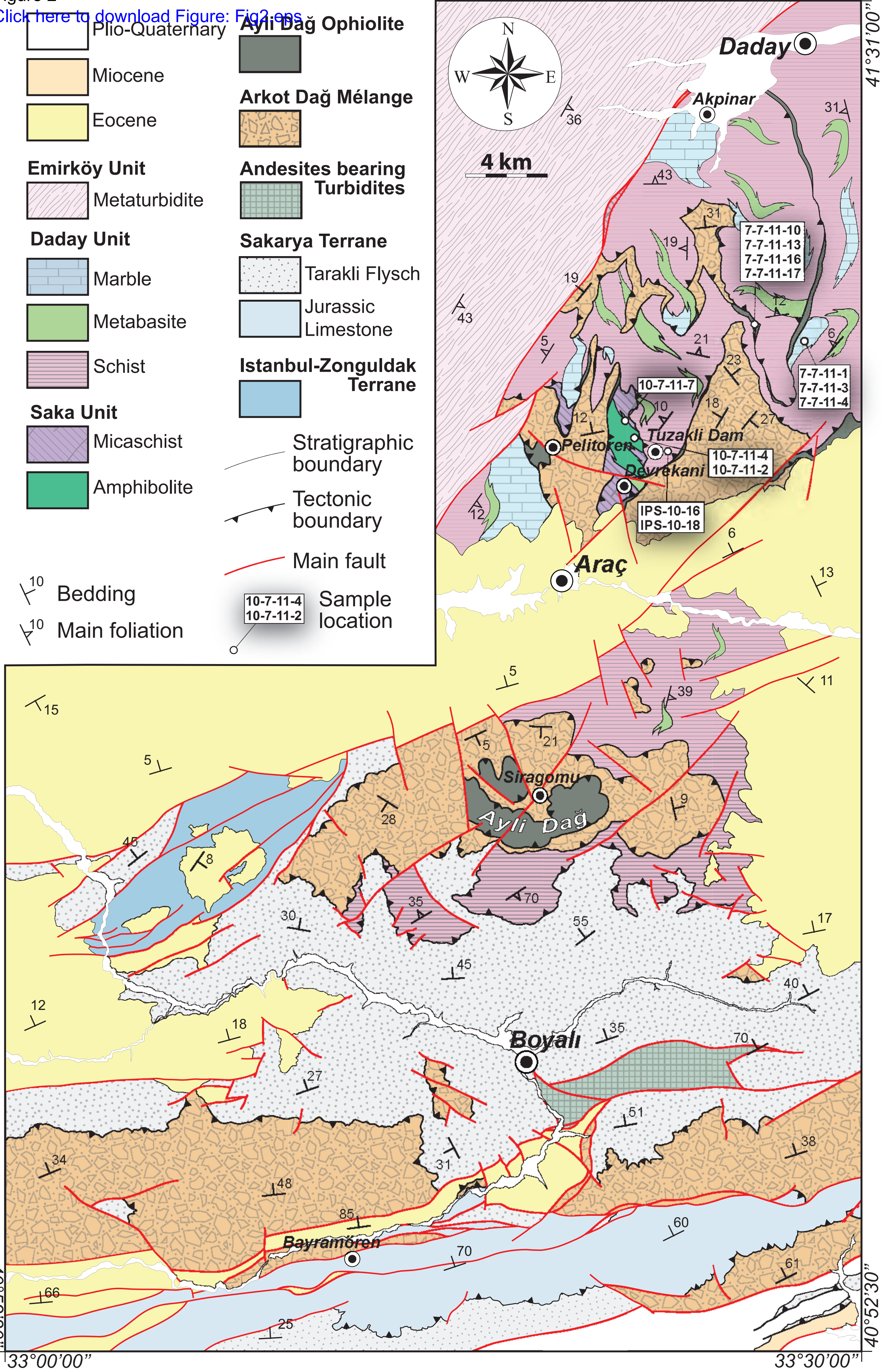

Figure 3
Click here to download Figure: Fig3.eps

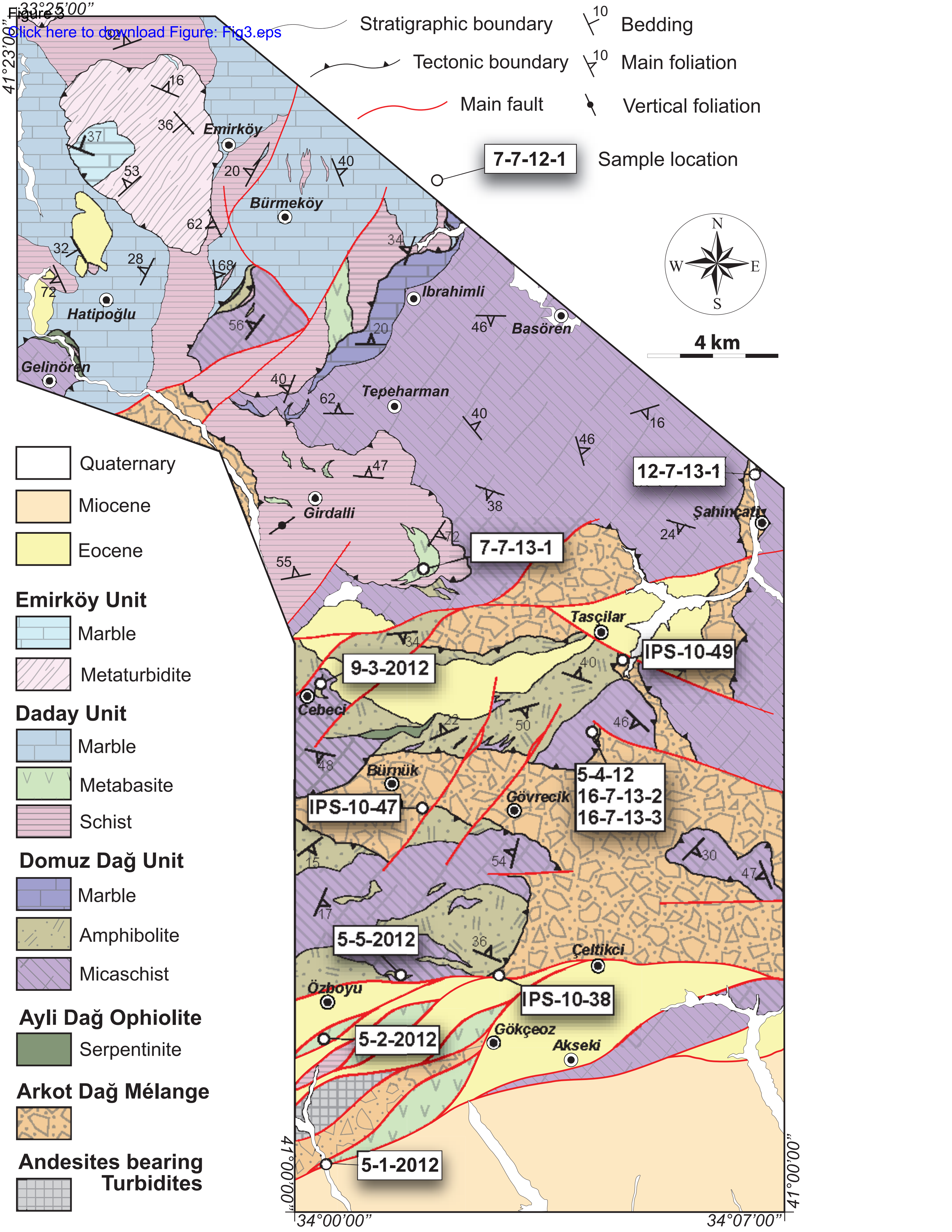

Figure 4

Click here to download Figure: Fig4.eps

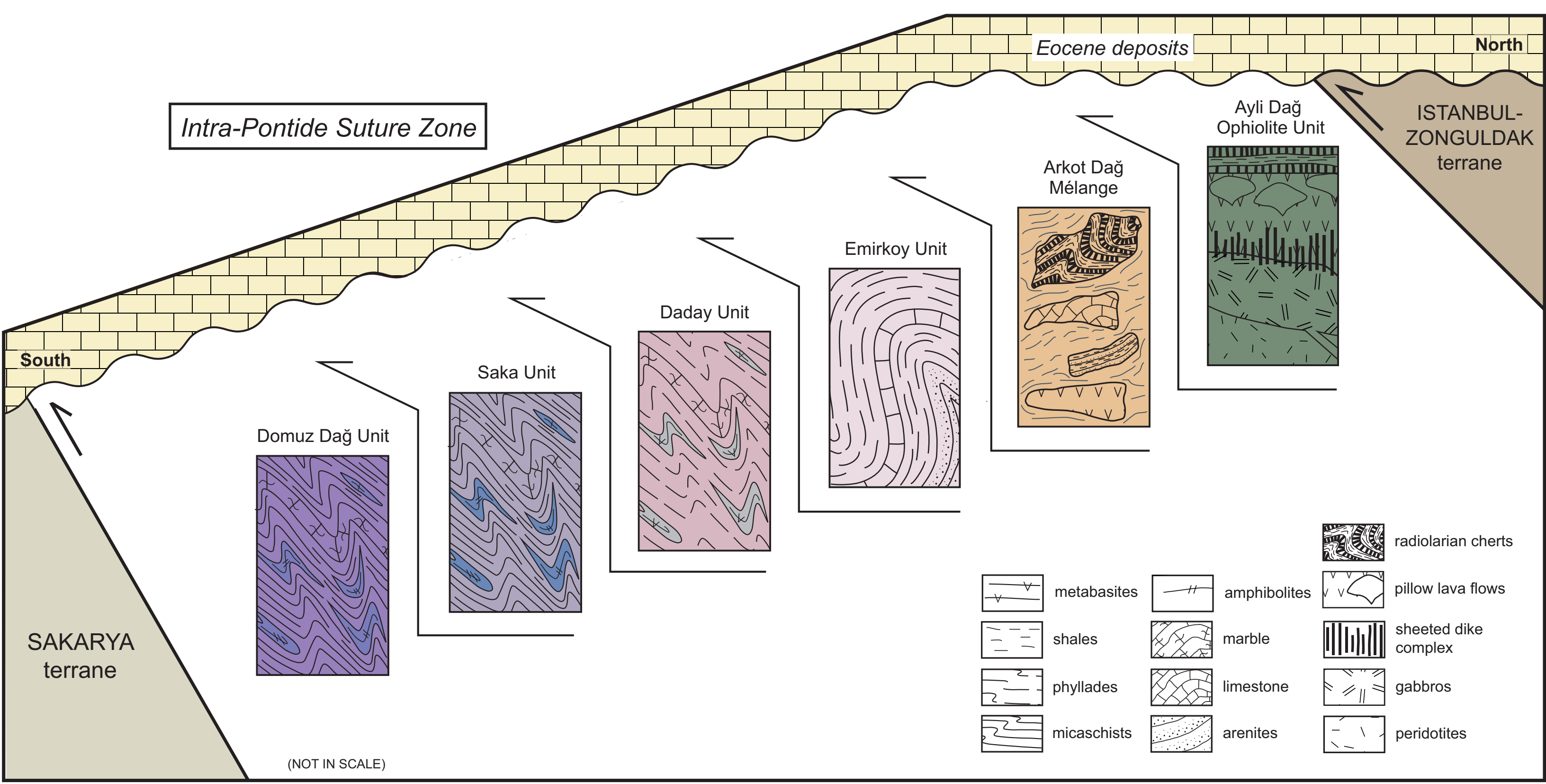

Figure 5

Click here to download Figure: Fig5.eps

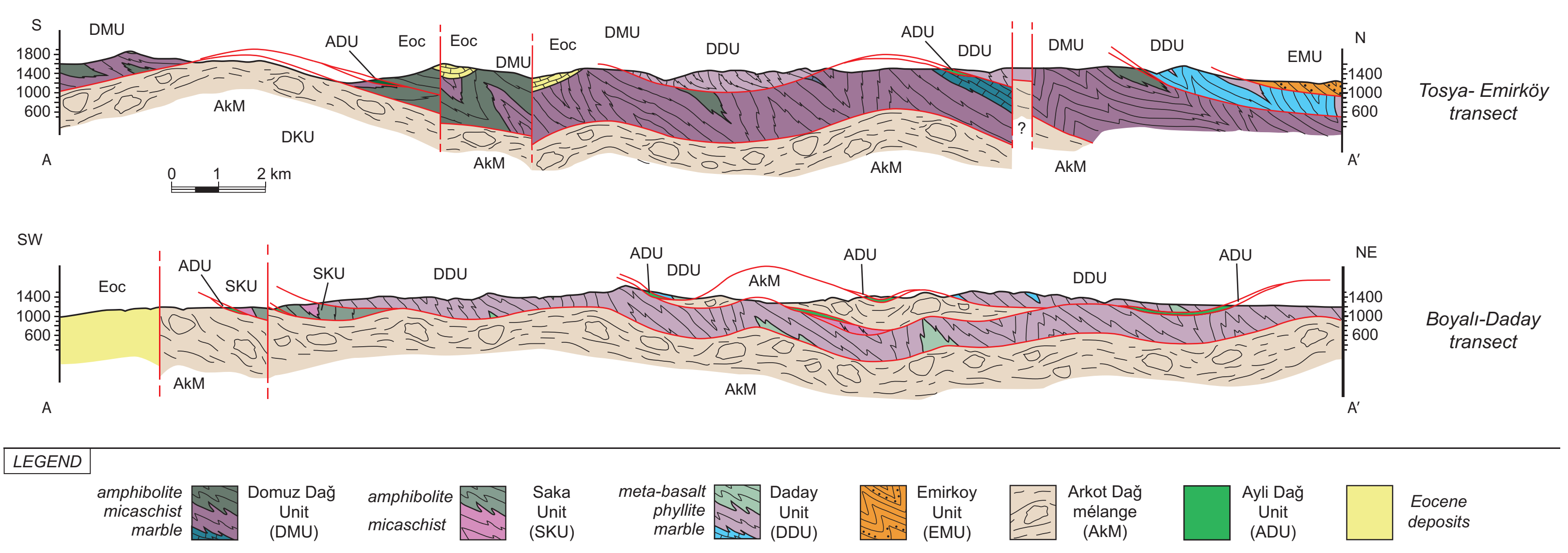

Figure 6
Click here to download Figure: Fig6.eps

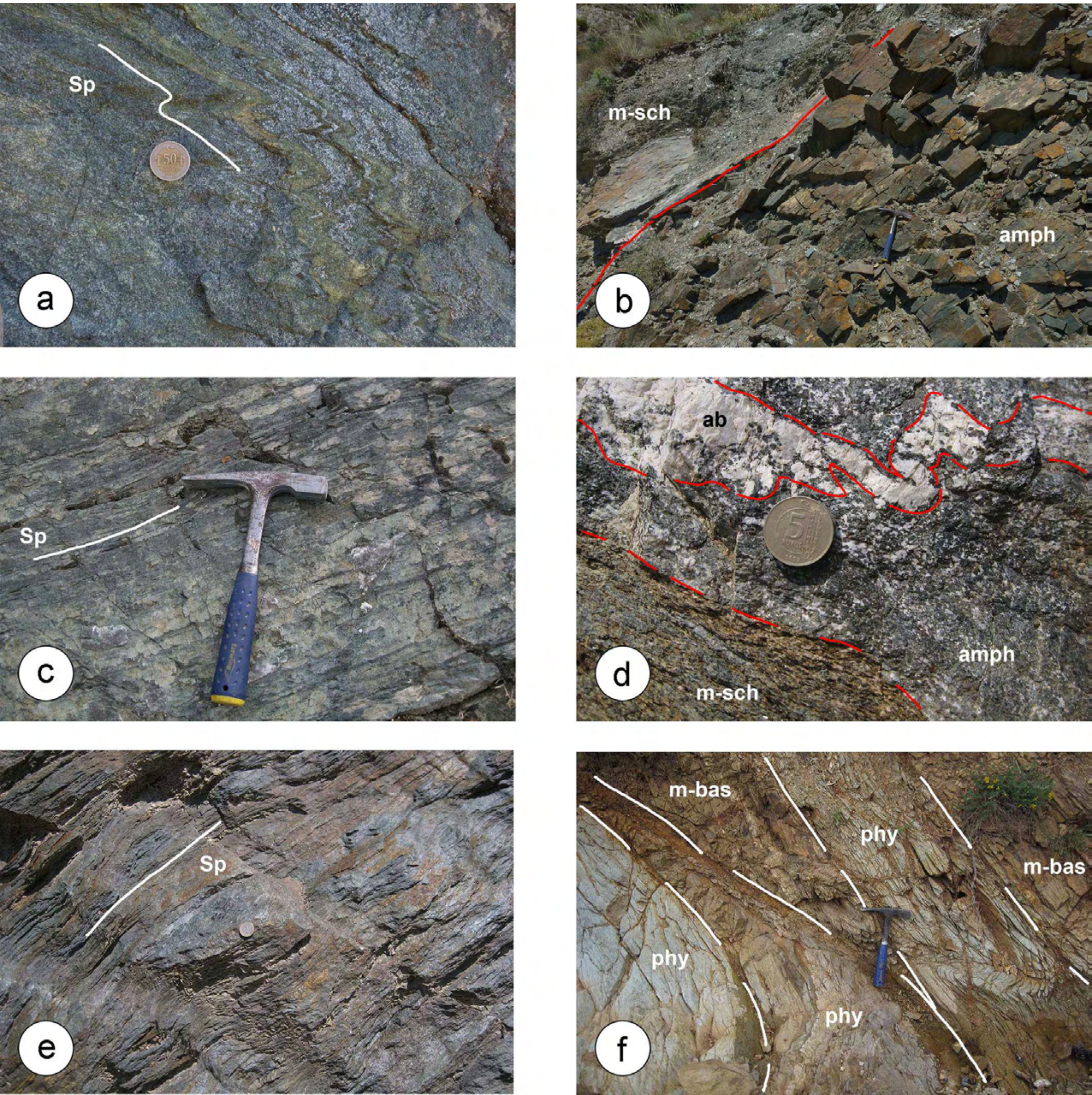

Figure 7
Click here to download Figure: Fig7.eps

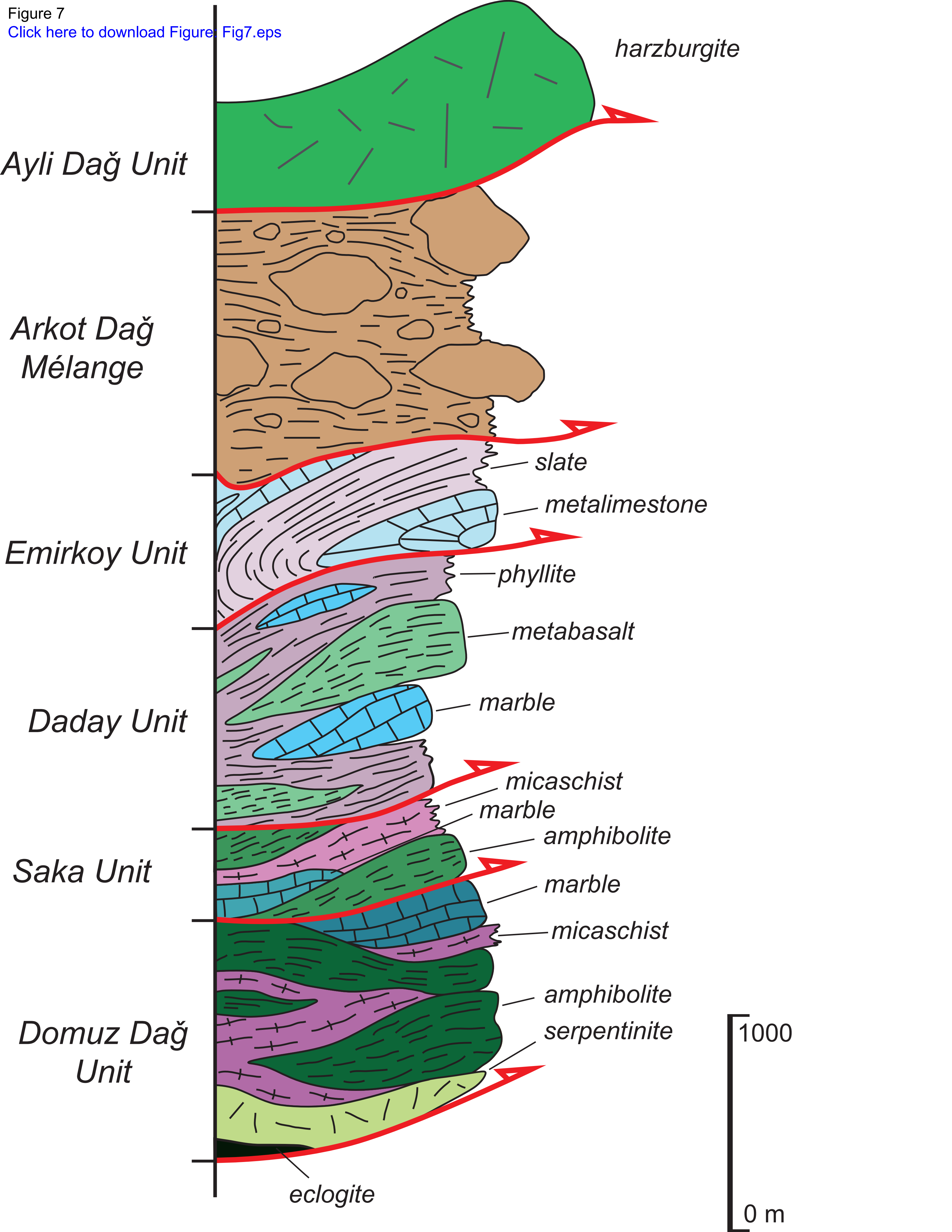

Figure 8
Click here to download Figure: Fig8.eps

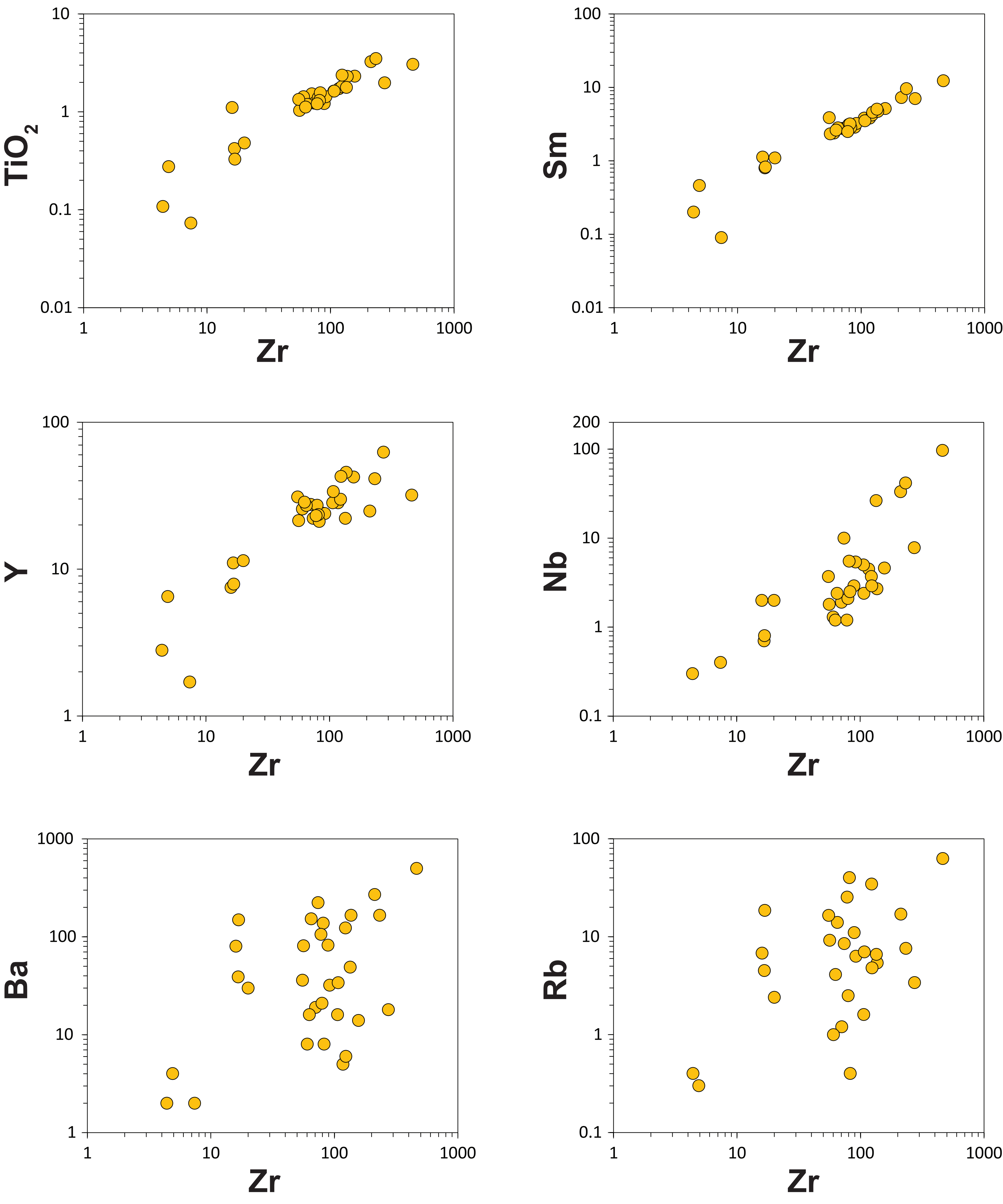

Figure 9

Click here to download Figure: Fig9.eps

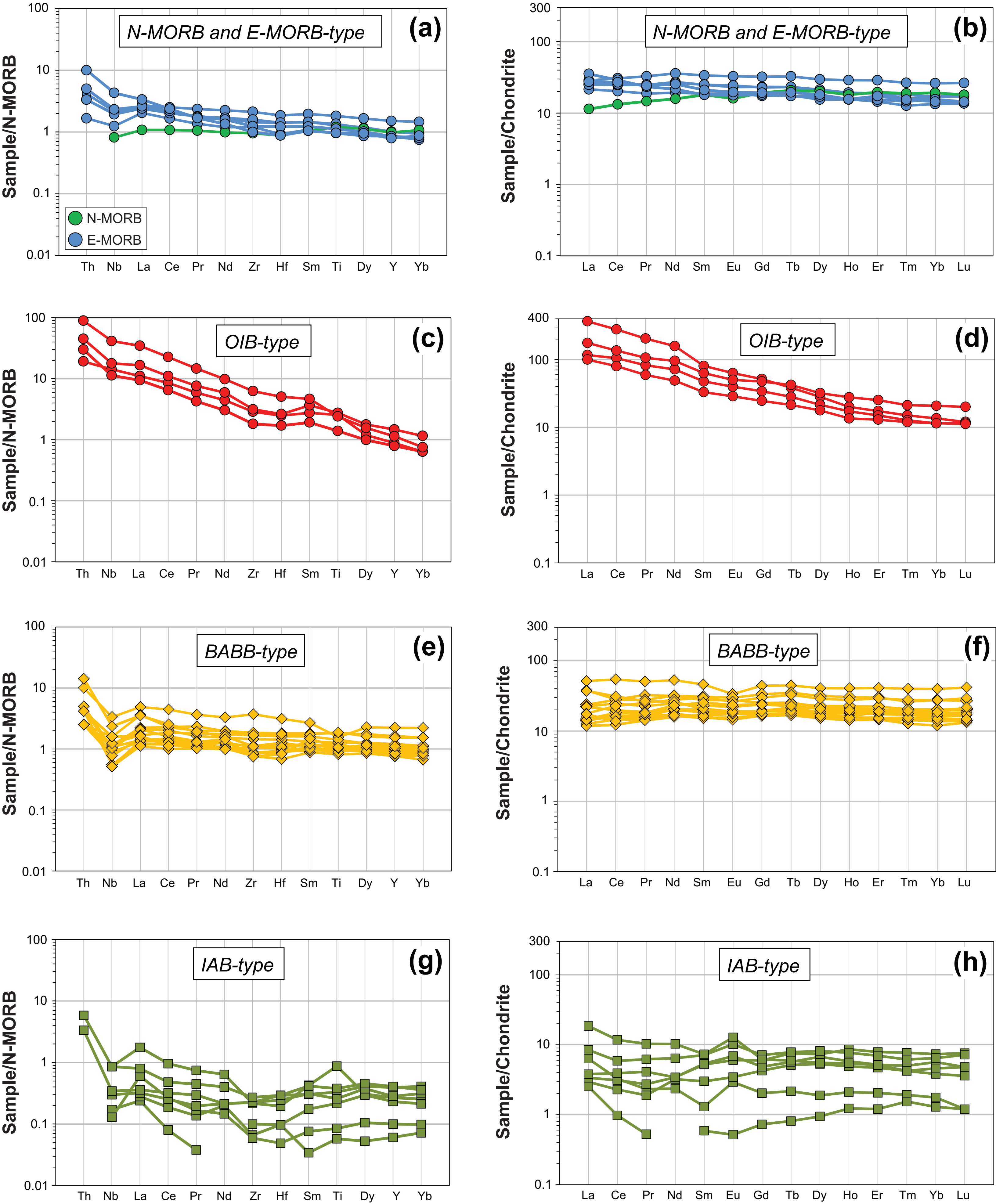

Figure 10

Click here to download Figure: Fig10.eps

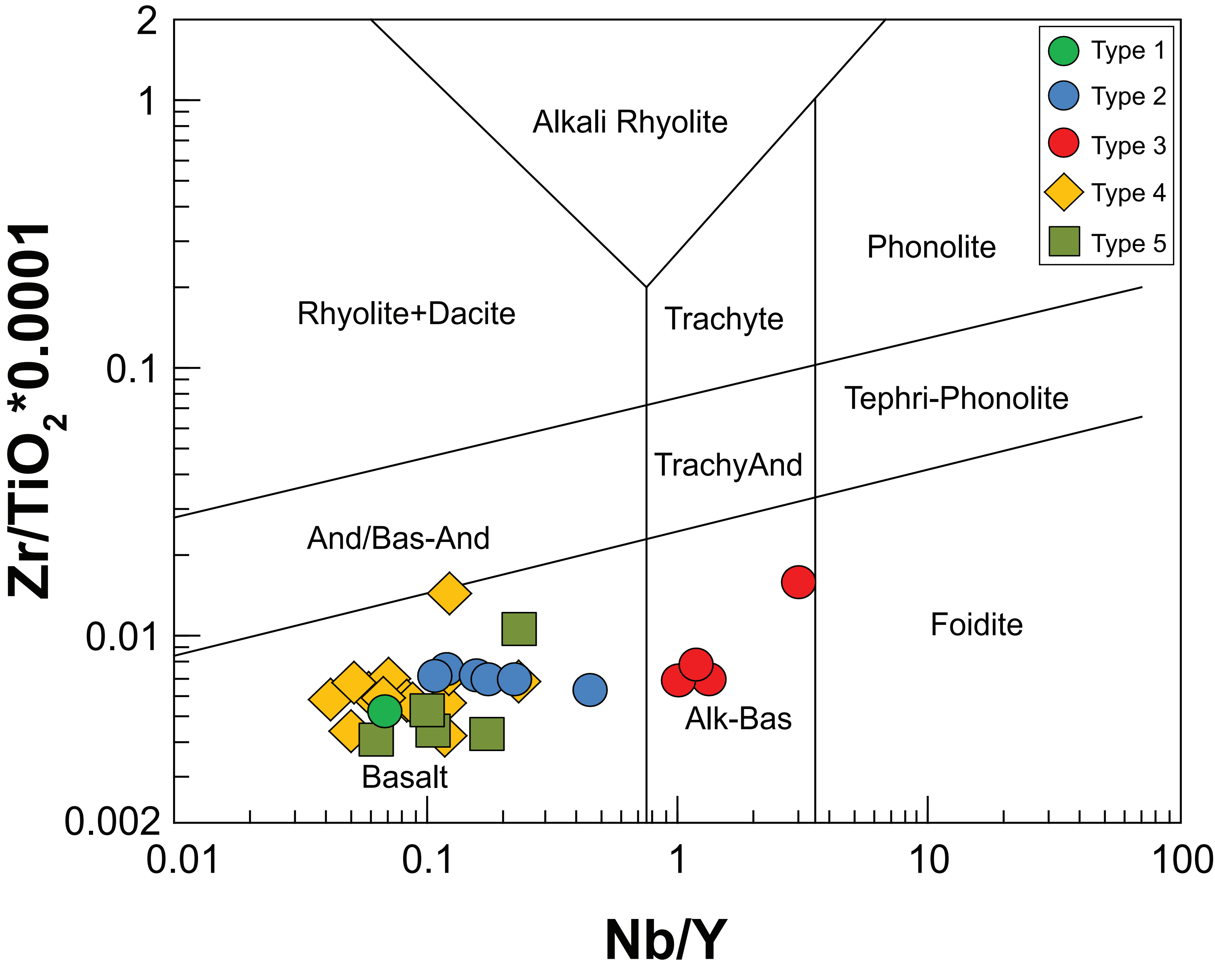

Figure 11

Click here to download Figure: Fig11.eps

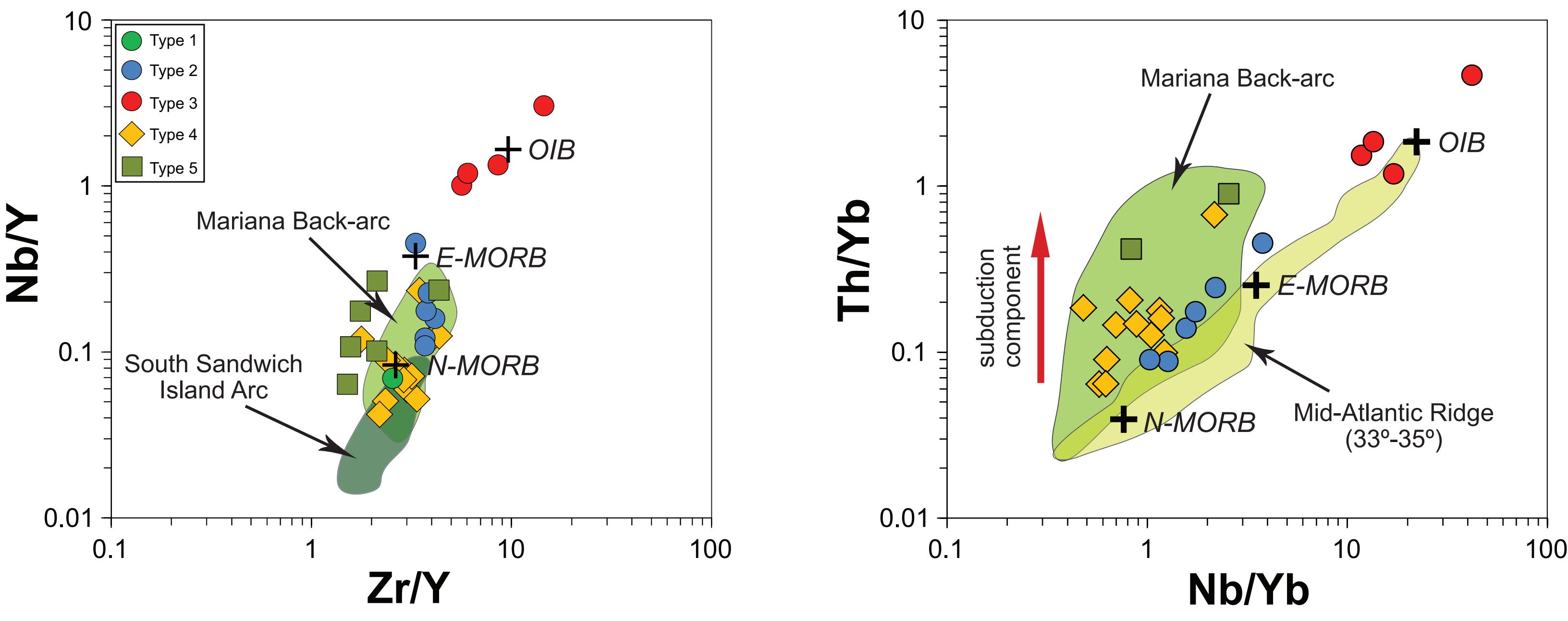

Figure 12

Click here to download Figure: Fig12.eps

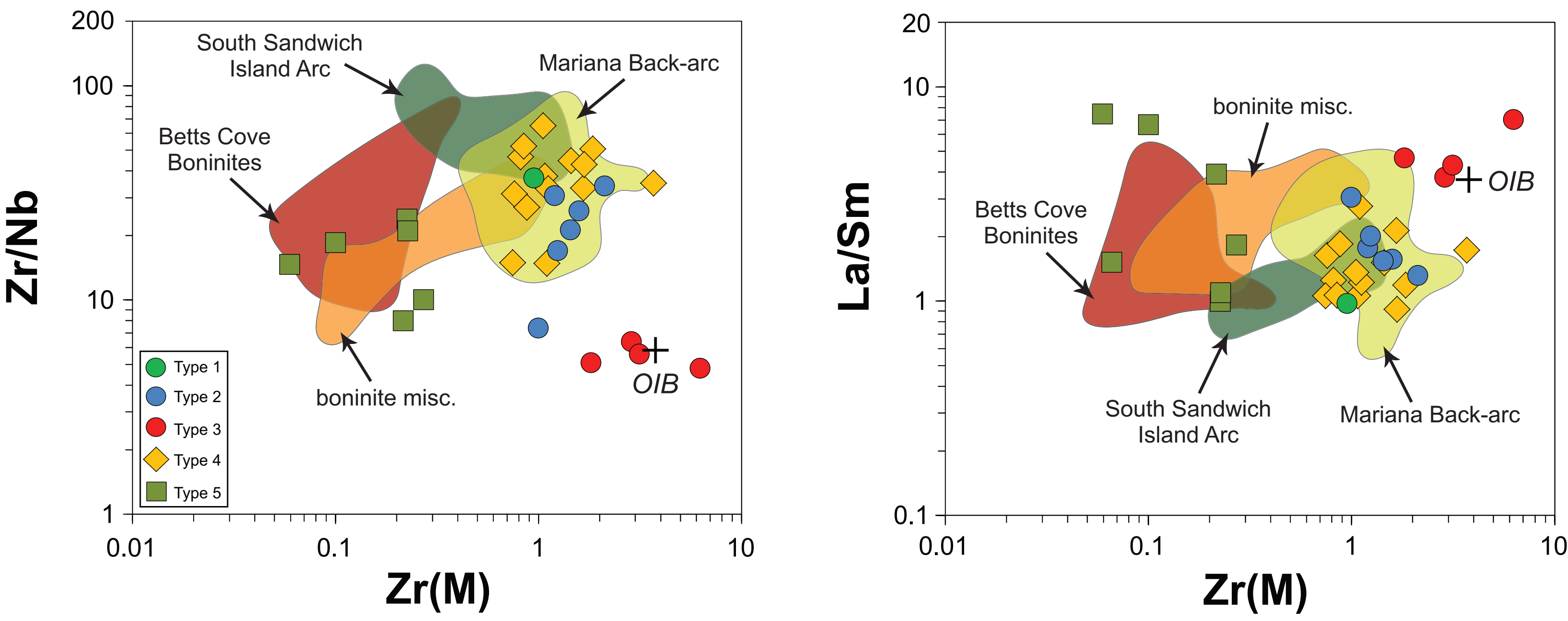

Figure 13

Click here to download Figure: Fig13.eps

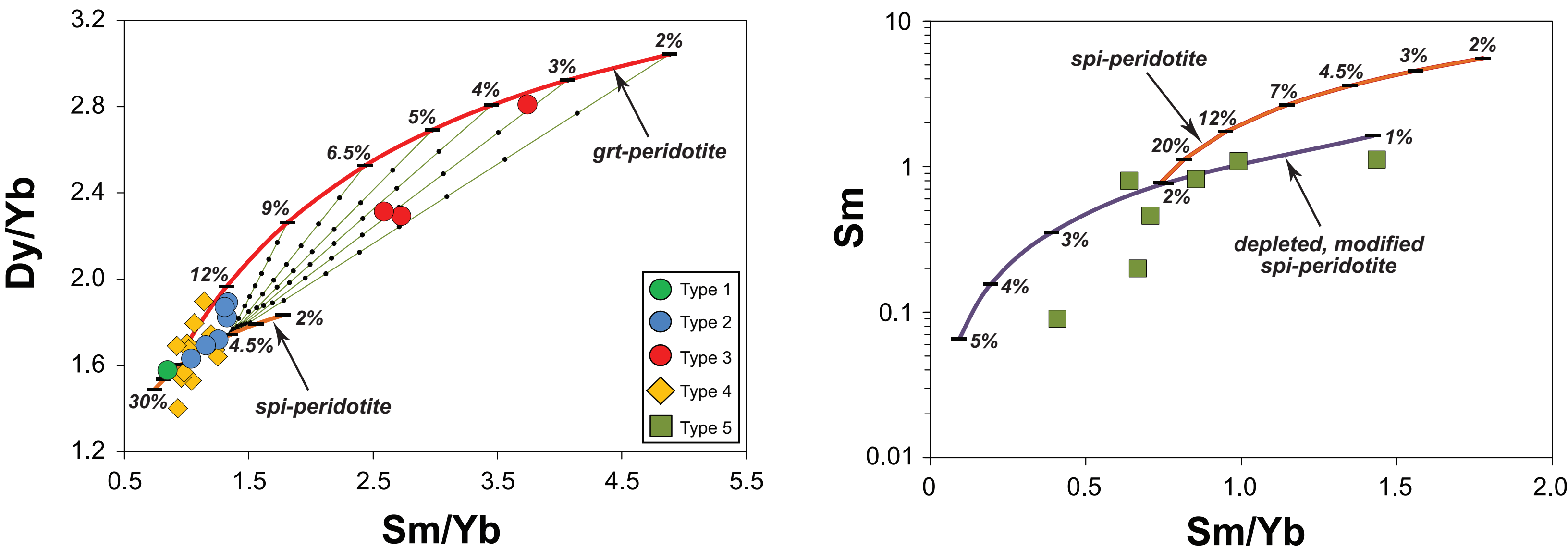

Figure 14
Click here to download Figure: Fig14.eps

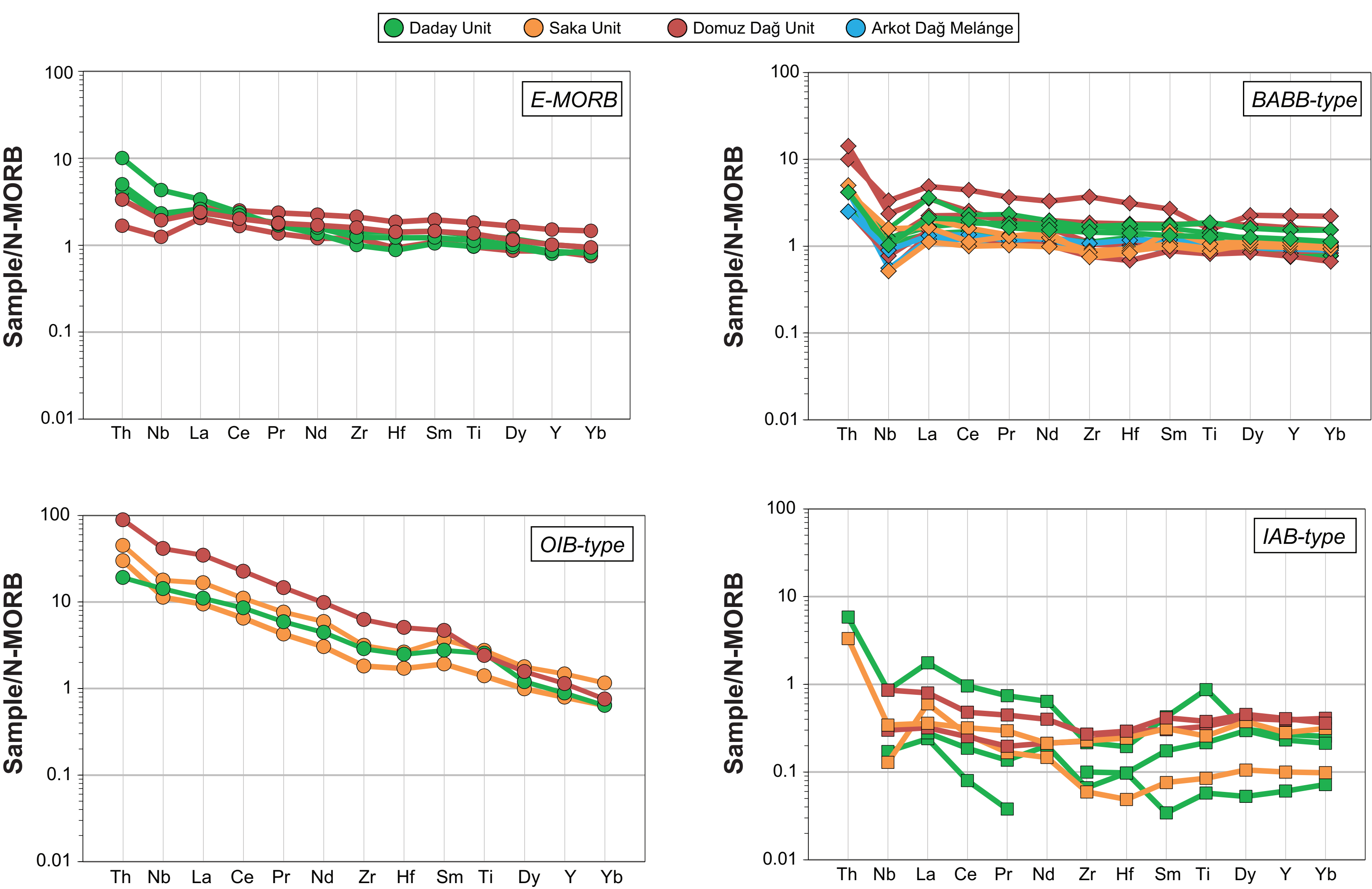

Figure 15
Click here to download Figure: Fig15.eps

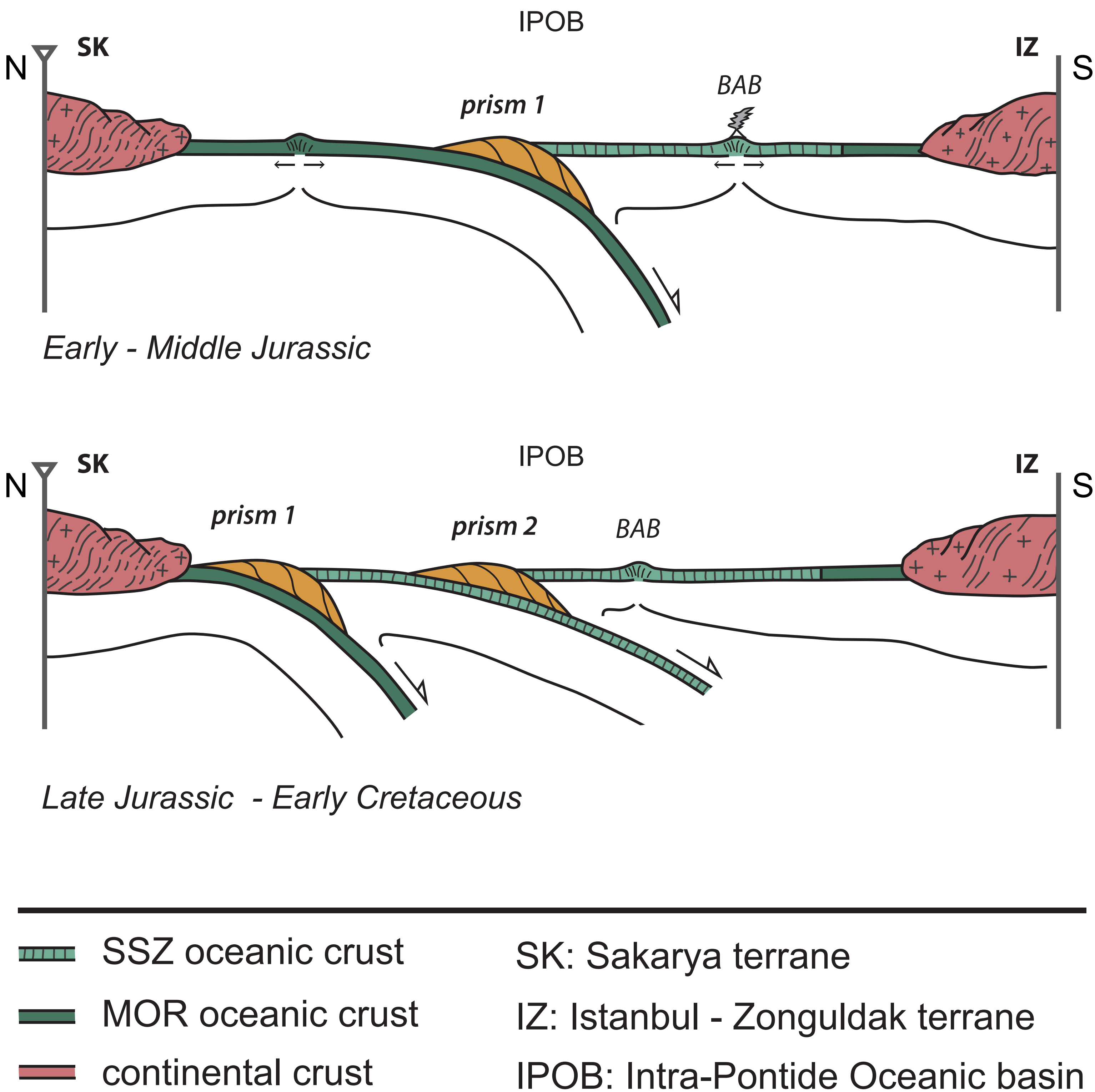

Table 1

GEOLOGICAL MAP-BASED CORRELATION			
Present Study	**Ustaömer and Robertson 1999**	**Okay et al. 2006**	**Okay et al. 2013**
Daday Unit	part of Domuzdag-Saraycikdag Complex	part of Late Cret. Acc. Complex	part of Saka, Esenler and Domuzdag Complexes
Saka Unit	-	part of Late Cret. Acc. Complex	part of Saka Complex
Domuzdag Unit	part of Domuzdag-Saraycikdag Complex	part of Domuzdag Complex	part of Domuzdag Complex
Emirkoy Unit	-	part of Late Cret. Acc. Complex	part of Martin and Esenler Complexes

LITHOLOGY-METAMORPHISM-BASED CORRELATION			
Present Study	**Ustaömer and Robertson 1999**	**Okay et al. 2006**	**Okay et al. 2013**
Daday Unit	partly Domuzdag-Saraycikdag Complex	partly Domuzdag Complex	partly Martin, Esenler and Domuzdag Complexes
Saka Unit	-	-	Saka Complex
Domuzdag Unit	partly Domuzdag-Saraycikdag Complex	partly Domuzdag Complex	partly Domuzdag Complex
Emirkoy Unit	partly Domuzdag-Saraycikdag Complex	-	-

Table 2

Unit						Daday	
Type	**2**	**2**	**4**	**4**	**4**	**4**	**3**
Sample	IPS-10-54	IPS-10-56	IPS-10-52	IPS-10-16	7-7-13-1	IPS-10-18	5-1-2012
SiO2	46.28	47.36	46.89	43.07	49.84	44.34	44.01
Al2O3	15.58	14.46	14.21	20.64	15.01	11.49	13.72
Fe2O3	10.27	8.83	10.18	12.03	11.41	12.73	12.72
MgO	7.59	8.06	6.46	3.49	6.05	5.94	8.44
CaO	10.1	8.96	10.57	9.65	6.96	11.47	9.89
Na2O	3.31	4.13	4.19	2.96	4.43	1.21	2.14
K2O	0.1	0.37	0.06	1.46	0.37	0.11	1.12
TiO2	1.55	1.34	1.48	1.72	1.56	2.13	3.11
P2O5	0.15	0.14	0.12	0.15	0.13	0.19	0.38
MnO	0.15	0.14	0.19	0.14	0.17	0.23	0.16
Cr2O3	0.054	0.051	0.046	0.076	0.003	0.026	0.016
LOI	4.6	5.9	5.4	4.4	3.9	9.9	4.0
Sum	99.76	99.79	99.82	99.79	99.82	99.78	99.68
Ni	104.2	104.2	56.6	149.9	7.0	40.8	57.3
Sc	37	32	47	45	36	40	33
V	265	219	274	230	314	381	312
Co	46.4	36.2	47.4	54.6	33.6	37.6	46.7
Ba	16	32	8	123	34	6	270
Rb	1.6	6.3	0.4	34.5	7.0	4.8	17.0
Sr	337.6	190.5	64.2	564.2	105.4	276.2	272.5
U	0.1	0.4	b.d.	0.6	0.1	0.2	0.7
Pb	1.2	0.4	0.5	1.8	0.2	2	0.3
Th	0.5	0.6	0.3	0.3	0.5	0.3	2.3
Hf	2.9	2.5	2.6	3.3	2.9	3.6	5.1
Nb	5	5.4	2.5	3.7	2.4	2.9	33.2
Ta	0.3	0.4	0.2	0.2	0.1	0.2	2.1
Zr	106.2	91.9	82.8	123.3	107.4	124.2	212.8
Y	28.3	23.9	21.1	29.9	33.7	42.8	24.8
La	5.9	6.5	3.5	9	5.3	4.2	27.6
Ce	15.5	16.5	11.1	17.2	15.1	13.9	64.1
Pr	2.38	2.31	1.7	3.09	2.15	2.39	7.80
Nd	12.4	11.9	9.2	14.7	11.5	13	33.4
Sm	3.82	3.22	2.85	4.21	3.50	4.58	7.26
Eu	1.41	1.14	1.13	1.59	1.28	1.52	2.30
Gd	4.71	3.96	3.54	5.16	4.90	6.16	7.00
Tb	0.86	0.72	0.66	0.94	0.91	1.21	1.04
Dy	5.41	4.6	4.15	5.57	5.76	7.32	5.45
Ho	1.1	0.89	0.83	1.21	1.29	1.58	0.98
Er	3.13	2.88	2.45	3.36	3.70	4.84	2.48
Tm	0.47	0.4	0.37	0.5	0.53	0.72	0.33
Yb	2.86	2.46	2.38	3.03	3.44	4.67	1.94
Lu	0.45	0.36	0.35	0.46	0.52	0.73	0.29

							Saka
5	***5***	***5***	***2***	***4***	***4***	***4***	***3***
7-7-11-4	7-7-11-1	7-7-11-3	5-2-2012	7-7-11-13	7-7-11-10	10-7-11-7	10-7-11-4
44.71	49.38	51.05	47.38	49.69	45.19	45.05	42.40
18.94	4.89	4.52	15.65	15.05	14.91	16.37	13.63
9.11	7.74	7.43	10.89	11.36	12.98	10.68	17.18
7.01	21.37	17.04	8.14	7.61	12.04	6.44	6.26
10.89	11.59	16.83	9.34	9.26	8.77	14.42	10.16
2.48	0.31	0.46	3.22	2.67	1.31	3.04	3.07
0.37	0.04	0.05	0.34	1.19	0.73	0.29	0.85
1.05	0.07	0.27	1.18	1.17	1.31	1.09	3.43
0.04	<0.01	<0.01	0.11	0.12	0.09	0.10	0.65
0.15	0.15	0.16	0.17	0.22	0.35	0.14	0.25
0.013	0.104	0.440	0.034	0.033	0.102	0.065	0.012
5.0	3.9	1.3	3.3	1.4	1.9	2.1	1.8
99.80	99.60	99.59	99.75	99.82	99.71	99.85	99.70
7.7	99.2	63.6	58.4	33.8	76.7	16.3	25.6
43	53	82	45	40	49	37	37
279	229	274	259	295	343	282	413
30.6	47.6	44.7	41.6	39.5	50.4	45.6	53.1
80	2	4	223	153	36	16	166
6.8	b.d.	0.3	8.5	14.0	16.5	4.1	7.6
266.0	7.0	10.8	276.6	129.9	14.8	336.4	316.0
0.2	b.d.	b.d.	0.2	0.3	b.d.	0.1	0.9
1.0	0.2	0.2	0.2	1.2	0.3	0.5	0.9
0.7	b.d.	b.d.	1.2	0.6	0.5	b.d.	5.4
0.4	0.2	0.2	1.8	1.9	1.7	1.8	5.4
2.0	0.4	b.d.	10.0	2.4	3.7	1.2	41.6
0.1	b.d.	b.d.	0.7	0.2	0.3	0.1	2.8
16.0	7.4	4.9	73.9	65.0	55.3	62.8	233.0
7.5	1.7	6.5	22.2	27.1	31	28.6	41.2
4.4	0.6	0.7	8.4	5.2	4.1	2.8	41.6
7.2	0.6	1.4	17.8	12.1	8.4	7.5	82.8
0.98	0.05	0.18	2.22	1.77	1.72	1.35	10.08
4.8	<0.3	1.5	10.1	9.4	10.8	7.4	44.5
1.12	0.09	0.46	2.75	2.81	3.87	2.62	9.63
0.74	0.03	0.20	1.03	1.02	1.36	1.03	2.90
1.27	0.15	0.88	3.73	4.03	4.92	3.93	9.74
0.22	0.03	0.19	0.64	0.71	0.84	0.72	1.56
1.40	0.24	1.35	4.32	4.52	5.25	4.80	8.09
0.31	0.07	0.28	0.88	1.02	1.12	1.06	1.58
0.85	0.20	0.78	2.56	2.89	3.15	3.05	4.18
0.11	0.04	0.11	0.38	0.44	0.5	0.46	0.55
0.78	0.22	0.65	2.65	2.93	3.14	2.84	3.53
0.12	0.03	0.09	0.36	0.43	0.54	0.43	0.50

3	***5***	***5***	***2***	***2***	***2***	***4***	***4***
7-7-11-16	7-7-11-17	10-7-11-2	12-7-13-1	5-5-2012	5-8-2012	13-7-13-1	16-7-13-3
49.92	45.16	50.47	47.89	50.27	47.81	48.01	48.25
12.54	9.60	16.82	17.60	14.36	14.25	15.15	13.21
11.54	7.00	7.48	9.47	11.71	13.63	12.27	15.06
8.34	21.96	8.18	7.64	7.61	6.53	8.99	6.35
8.4	8.06	10	8.85	5.78	8.11	6.15	8.60
3.72	0.39	3.2	4.18	4.69	3.63	3.22	3.36
0.66	0.05	0.96	0.74	0.02	0.04	0.23	0.22
1.73	0.10	0.32	1.19	1.66	2.23	1.91	2.25
0.32	<0.01	0.02	0.12	0.13	0.18	0.28	0.15
0.33	0.18	0.12	0.16	0.18	0.20	0.30	0.22
0.101	0.185	0.079	0.044	0.029	0.012	0.020	0.011
2.1	6.8	2.1	1.8	3.3	3.1	3.2	2.1
99.76	99.63	99.81	99.75	99.79	99.74	99.70	99.77
88.6	297.2	35.5	48.1	38.5	28.3	30.6	28.4
24	23	33	34	45	44	37	46
165	75	132	225	282	385	252	434
51.7	57.6	38.1	39.8	40.7	42.8	32.3	45.4
49	2	149	82	5	14	18	166
6.6	0.4	18.6	11.0	b.d.	b.d.	3.4	5.4
118.7	34.0	178	204.8	105.6	138.7	166.4	112.9
1	b.d.	0.1	b.d.	0.1	b.d.	0.5	b.d.
2.1	0.2	1	0.7	0.2	0.2	0.5	0.1
3.6	b.d.	0.4	0.2	0.4	0.4	1.2	0.3
3.5	0.1	0.5	1.9	2.9	3.8	6.4	3.7
26.4	0.3	0.8	2.9	4.5	4.6	7.8	2.7
1.5	b.d.	b.d.	0.2	0.4	0.4	0.5	0.2
134.6	4.4	16.8	89.0	117.4	157.0	274.0	137.0
22.2	2.8	7.9	24.0	28.3	42.3	62.6	45.6
23.6	1.5	0.9	5.1	6.0	6.8	12.2	5.6
48.8	2.0	2.4	12.4	15.1	18.8	33.2	17.0
5.62	0.22	0.39	1.79	2.36	3.11	4.82	2.64
22.8	1.1	1.6	9.0	12.7	16.8	24.7	14.8
5.05	0.20	0.82	2.87	3.81	5.15	7.04	4.71
1.66	0.17	0.4	1.09	1.34	1.90	1.95	1.73
5.05	0.42	1	3.59	4.80	6.63	9.09	6.84
0.79	0.08	0.21	0.66	0.86	1.21	1.65	1.30
4.51	0.48	1.71	3.92	5.23	7.53	10.32	7.98
0.77	0.12	0.33	0.89	1.08	1.65	2.31	1.74
2.15	0.34	0.86	2.40	3.17	4.78	6.82	4.97
0.31	0.05	0.13	0.33	0.41	0.69	1.04	0.68
1.95	0.30	0.96	2.28	2.87	4.45	6.75	4.69
0.28	0.03	0.12	0.34	0.43	0.66	1.04	0.67

Domuzdag						*Arkotdag Melan*	
4	***4***	***4***	***3***	***5***	***5***	***1***	***4***
16-7-13-2	9-3-2012	IPS-13-05	4-13-2012	5-4-2012	4_8_2012	IPS-10-47	IPS-10-38
50.39	49.12	49.06	47.96	56.10	51.30	41.41	55.16
16.52	15.87	16.76	16.98	13.02	15.29	12.46	13.89
11.10	11.47	10.25	10.44	7.86	7.40	10.26	11.16
7.36	5.46	5.62	4.81	8.68	8.80	6.54	5.55
3.71	6.79	10.62	4.85	5.88	10.69	13.4	4.44
4.19	1.06	1.81	3.98	5.03	3.50	3.3	5.07
1.20	1.11	1.30	3.07	0.30	0.14	0.08	0.19
0.99	1.21	1.17	2.94	0.41	0.47	1.36	1.35
0.02	0.09	0.07	1.02	0.01	0.02	0.11	0.15
0.24	0.20	0.23	0.12	0.10	0.14	0.17	0.15
0.024	0.037	0.046	0.003	0.046	0.025	0.035	0.02
4.0	7.4	2.8	3.5	2.4	2.0	10.7	2.7
99.80	99.81	99.78	99.64	99.81	99.80	99.82	99.83
36.1	105.8	33.2	16.8	47.9	27.9	50.7	10.3
37	34	42	16	35	39	41	29
322	223	260	145	223	204	319	265
32.2	53.6	38.1	25.4	34.2	34.3	39.9	25.9
81	138	106	499	39	30	19	21
9.2	40.1	25.4	63.0	4.5	2.4	1.2	2.5
84.2	137.0	369.4	672.6	70.9	151.1	108.2	78.2
b.d.	0.5	b.d.	2.2	b.d.	b.d.	1	0.3
0.3	1.6	1.1	1.1	0.4	0.2	0.9	0.7
0.3	1.7	b.d.	10.7	b.d.	b.d.	b.d.	0.3
1.4	2.2	2.1	10.4	0.6	0.6	1.8	2.4
1.8	5.5	1.2	96.6	0.7	2.0	1.9	2.1
b.d.	0.4	0.1	5.9	b.d.	b.d.	0.1	0.1
56.3	81.5	78.0	463.7	16.7	20.1	70.5	79.5
21.4	23.5	23.1	31.9	11.0	11.4	27.6	27.2
3.8	8.8	3.4	86.7	0.8	2.0	2.7	3.3
9.4	19.0	9.8	170.1	1.9	3.6	8.1	10.2
1.46	2.52	1.63	19.36	0.26	0.59	1.39	1.53
7.7	12.1	7.8	73.7	1.6	3.0	7.4	9.5
2.32	3.17	2.49	12.30	0.80	1.09	2.76	3.11
0.91	1.09	1.03	3.65	0.35	0.59	0.93	1.03
3.38	3.94	3.53	10.60	1.23	1.47	3.97	3.99
0.62	0.71	0.66	1.42	0.28	0.29	0.77	0.8
3.85	4.15	4.20	7.13	1.86	2.07	5.14	4.68
0.81	0.88	0.89	1.14	0.49	0.44	1.03	1.08
2.42	2.53	2.55	2.88	1.31	1.16	3.25	3.24
0.33	0.40	0.38	0.39	0.20	0.16	0.49	0.49
2.03	2.53	2.34	2.30	1.25	1.10	3.26	3.34
0.33	0.37	0.35	0.30	0.19	0.18	0.45	0.5

ge
4
IPS-10-49
54.01
14.46
12.86
4.03
4.06
5.51
0.12
1.38
0.1
0.17
0.018
3.1
99.86
11.7
34
419
43.1
8
1
63.7
0.2
2.7
0.5
2
1.3
b.d.
60.5
25.7
3
8.9
1.37
8.3
2.39
0.84
3.41
0.67
4.34
0.92
3.08
0.44
2.71
0.42